Dual Active Contour Models for Segmentation: Survey on Level Set and Variational Formulations

Authors

Italo Messias Felix Santos(1), Gastão Florêncio Miranda Junior(1), Paulo Sérgio Silva Rodrigues(2), Gilson Antonio Giraldi(3)

Affiliations

(1) Federal University of Sergipe, Sergipe, Brazil;
(2) Centro Universitário FEI, São Bernardo do Campo, Brazil;
(3) National Laboratory for Scientific Computing, Petrópolis, Brazil.

Correspondence

Gilson Antonio Giraldi

National Laboratory for Scientific Computing, Petrópolis, Brazil.

Email: gilson@lncc.br

Abstract

Dual snake models are powerful techniques for boundary extraction and segmentation of medical and biological images. In these methods the key idea is: one contour contracts from outside the target and another one expands from inside as a balanced technique with the ability to reject local minima. Such approach was originally proposed in the context of parametric snakes. More recently, it was re-worked through implicit formulation where the deformable contours are zero level sets of embedding functions. In this paper we review implicit dual active contours for medical image segmentation. We start with a background in level set methods. Following, we consider variational formulations of dual models, aiming to set the background to derive the evolution scheme through the Euler-Lagrange equations, and to clarify the global optimization capabilities of dual techniques. Then, we summarize numerical aspects regarding finite difference approaches, initial and boundary conditions for dual techniques. Following, we review variational implicit models which are very influenced by the Chan-Vese Active contour model. Next, non-variational approaches are described, where the governing equations are not explicit derived from Euler-Lagrange expressions. We survey applications for shape recovery in transmission electron microscopy, computed tomographic (CT), and magnetic resonance imaging (MRI) modalities. We offer a discussion about important points that have emerged from this review and point out drawbacks of dual approaches. Besides, we present promising perspectives of dual active contour models and related topics for image segmentation.

1 Introduction

Segmentation is a fundamental step for image analysis and computer vision tasks involving object tracking and recognition [1, 2]. In digital image processing, segmentation aims to partition the set of pixels of an image into disjoint groups, each one corresponding to some uniform pattern with respect to a predefined criterion [3]. There are numerous methods focusing on image segmentation which can be roughly classified in region-based, edge-based, thresholding, clustering, and machine learning methods [4]. In this paper we focus on active contour models that fall into region-based and edge-based segmentation techniques categories. Edge-based models take local gradient information to enforce the active contour toward the desired object borderlines. Edge-based models have been successfully used for images with well defined object boundaries. However, these models are sensitive to noise and they strongly depend on the initial contour position. On the other hand, region-based active contour models usually apply region statistics information to steer the evolution of the active contour. Consequently, they are less sensitive to noise and can perform better than edge-based active contours for images with subjective edges.

Active contour models (ACM) are 2D deformable approaches, which includes the popular snake models proposed by Kass at al. [5]. They can be described such as an elastic curve which can dynamically conform to object shapes in response to both internal (elastic) forces and external (image and constraint) forces that can be based on local information or derived from an energy optimization process [6, 7]. ACM models can be extended to 3D for boundary extraction in volume images, generating the so called deformable surfaces [8, 9]. ACM techniques can be classified as parametric or implicit ones. In the former, the deformable curve is described using some functional representation based on curve spaces or splines [10]. On the other hand, implicit ACMs, formulated through the level set technique, consist of embedding the deformable curve as the zero level set of a higher dimensional function and to solve the corresponding partial differential equation of motion [11, 12]. In the last decades, ACM approaches have been successfully applied for image segmentation and object tracking in computer vision and image analysis tasks in a wide range of applications [13, 14]. Their mathematical formulation makes easier to integrate image data, an initial estimated, desired contour properties and knowledge-based constraints, in a single extraction process [6, 15], for segmentation of both 2D or 3D images, being the former the focus of this paper.

Level set based models are more convenient than their parametric counterpart for recovering objects with unknown topologies because parametric models can not deal with topological changes without extra machinery [16, 17]. One of the well-known and most influential region-based active contour methods is the Chan-Vese model which is based on level set and Mumford-Shah functional for segmentation [18]. Despite of its

capabilities, the Chan-Vese model assumes that the image domain is the union of (almost) homogeneous regions. The local binary fitting energy (LBF) model generalizes the Chan-Vese technique and can handle images with intensity inhomogeneity better than its counterpart [19].

However, both implicit and parametric models are sensitive to the initial contour position due to artifacts, noise as well as inhomogeneities in the image field, that is responsible for the known non-convexity (local minima) of the ACM energy functional. To address this limitation some authors have proposed dual ACM methods [20]. The basic idea of the dual ACM is to reject local minima by using two contours: one which contracts from outside the target and one which expands from inside. Such proposal started in the area of parametric snakes [21, 22]. It makes possible to reduce the sensitivity to initialization through the comparison between the two snakes energy and positions. The two contours are interlinked to provide a methodology to carry the ACM out of local minima, which makes the solution less sensitive to initial contour position [20].

In [6] some of us present the Dual-Level-Set, an implicit formulation for dual snakes, based on the level set approach. The key idea of that work is to view the inner/outer contours as a level set of a suitable embedding function. If the corresponding surface evolves such that the two contours get closer, we can obtain the same behavior of parametric dual models by comparing inner and outer contour features. Besides, almost at the same time, the work [23] proposed a dual geometric active contour method that utilizes the Chan-Vese model to evolve each curve. Likewise [6], this model keeps implicit representation for the dual contours but now using two different level set functions.

Since the works presented in [6, 23], several dual ACM models based on level set formulation have been reported in the literature. In this way, we should mention the review [22], which summarizes remarkable parametric and implicit dual snake models known at that time. So, in order to avoid unnecessary redundancies with the survey [22], we have assembled a list of dual ACM models that, up to the best of our knowledge, completes the set of representative works in the area [6, 23, 24, 25, 26, 27, 28, 29, 30, 31, 32]. However, we review the Dual-Level-Set [6] and the dual geometric active contour method [23] once they started the idea of embedding dual snakes into the level set approaches. Henceforth, before going ahead, we shall distinguish between non-variational and variational level set formulation classes. In the former, the dual techniques represent each contour as a level set whose governing equation is not explicit derived from the associated Euler-Lagrange expressions, like is performed in the variational formulation category. Also, in order to avoid confusion with other areas, we must be careful about the term ’dual formulation’, that also appears in variational approaches but outside the scope of dual ACMs, meaning rewrite the optimization problem in the dual variables space (see [33] for an interesting application of such approach for image restoration). Moreover, we find also

the paper [34] that uses a dual self-organizing map approach to learn the object of interest and the background independently in order to guide a level set ACM, evolved through the lattice Boltzmann method, to complete the segmentation. Once the pre-processing is performed by a dual approach but the ACM is single, we do not describe the model [34] in this survey.

The remaining of the text is organized as follows. Section 2 presents an overview of the focused techniques. The level set method is described in section 3. Section 4 offers the variational background for the material. Section 5 gives details about numerical implementation of dual models. Following, in section 6 we describe the variational formulations for implicit dual ACMs with focus for medical image segmentation. Next, section 7 presents the non-variational dual approaches. We offer discussions on section 8 about important issues in the presented methods and point out drawbacks of dual approaches. In section 9 we present conclusions and final remarks.

2 Overview of Dual Models

Following the dual ACM methodology, the inner (or outer) zero level set is selected to evolve based on its governing equation. After convergence we check the contours similarity. If inner/outer contours are far from one each other then another zero level set will be chosen to evolve. This process will continue until one level set superposes the other. Dual level set models have been applied for medical image segmentation in, chest computed tomographic (CT) image slices [32], computed tomographic colonography (CTC) images [24], bone segmentation in high resolution peripheral quantitative computed tomography (HR-pQCT) [26], 3D segmentation in CT volumes [29], and magnetic resonance imaging (MRI) modalities [35, 31]. Moreover, live cell microscopy imaging, that is a key component in the biological research tasks, is another potential application field for dual snakes [27, 28].

Following a chronological order, the work [24] presents a variational dual level set model to segment the volumetric colon wall from computed tomographic colonography (CTC) images to automatically detect colonic polyps. In a pre-processing stage, tagged materials in CTC images were automatically removed via the partial volume based electronic colon cleansing strategy [36]. It is important to emphasize that the pre-processing stage is a fundamental step before application of active contour models in general. Despite of the fact that we have two contours collaborating in the process of searching the curve space for seeking the solution, the pre-processing stage makes smoother the landscape energy profile, improving the performance of each component of the dual model.

The pre-processing step for dual models has been implemented using traditional low-pass and high-pass filters, wavelets, thresholding, morphological operations, and fuzzy techniques [22, 17, 27, 32]. Besides, we can incorporate human-computer interaction methods to select a set of pre-defined points around the region of

interest. In [37] it is proposed a segmentation model that uses this idea, as well as gradient information, to guide a (single) active contour to the boundary of the object of interest.

Hence, inspired in [37, 19] the work [25] presents a dual level set technique in which one curve is used to seek the segmentation of all boundaries and the other to focus on the selected target in order to fulfill the geometric constraints. In this way, local and global region information are integrated, which allows to deal more efficiently with intensity inhomogeneity, weak edges and low contrast.

Image intensity inhomogeneity and noise level are hard problems for classical active contour models, mainly in medical image segmentation where complex structures with unknown geometries must be reconstructed. Among the ACM variants to address such issues, the approach proposed in [26] uses dual deformable curves, evolving based on level set method, to minimize a shared energy during the segmentation process. The technique follows the work [38] and uses local region information along the contour to compute the energy functional for cortical and trabecular bone segmentation in HR-pQCT data.

Dual ACM techniques are particularly useful when the topology of the target structure is a 2D torus like. For instance, transmission electron microscopy of insulin granules contains round organelles with a dense core, surrounded by a halo, which can vary in intensity and texture. Hence, in [27, 28] it is proposed a segmentation pipeline that uses a dual level set active contour for refining segmentation on each granule. The method applies the dual geometric active contour method presented in [23] and adds a locally fitting energy defined in [39] along with the smoothing term and signed distance regularizer for the level sets that represent the inner and outer contours. The idea of using local features through the selection of a set of points nearby the boundary combined with gradient information is used also in the dual formulation presented in [29] that includes terms to automatically scale level set functions to avoid re-initialization.

In [30], authors proposed a dual level set formulation based on the geodesic active contours model described in [40], to segment the bladder wall in magnetic resonance imaging (MRI). This model includes a balloon (inflation) force in the stopping criterion of the level set function for the inner wall and a spring model, that acts in between the inner and outer contours, in the governing equation of the outer wall implicit function.

The model presented in [31] can be viewed as a generalization of Chan-Vese ACM model that uses a dual approach to segment the four regions (gray matter, white matter, cerebrospinal fluid, and background) that appear in MRI diffusion weighed images. In [32] wavelet coefficients are used to compute the energies of different regions of chest CT images, and the inner/outer contours are defined by thresholding these fields. The active contour follows the Chan-Vese technique including a semi-automatic method to compute model parameters.

Among the summarized dual ACM models, the works [23, 24, 25, 26, 27, 28, 29, 31] belongs to the variational class while [30,32] are non-variational techniques. We shall add in this overview the non-variational method [6] that, together with [23], starts the idea of formulating dual snakes through level set.

3 Level Set Method in 2*D*

In this section we review some details of the ACM formulation based on level set approach [11]. As already explained, in ACM models an elastic curve undergoes deformations due to elastic (internal) and external forces derived from the image or constraints that restrict the curve evolution (see the video [41]). In this context, the main idea of level set method is to implicitly represent the deformable curve through an embedding function, also called level set function:

$$\phi: \mathbb{R}^2 \times \mathbb{R}^+ \to \mathbb{R}, \quad (1)$$

such that the contour, at $t = 0$, is given by the zero level set $S(t = 0)$:

$$S(0) = \{\boldsymbol{x} \in \mathbb{R}^2 | \phi(\boldsymbol{x}, 0) = 0\}. \quad (2)$$

The next step is to find an Eulerian formulation for the curve evolution. Following Sethian [11], let us suppose that the contour evolves in the normal direction with velocity $\boldsymbol{F}$ that may be a function of the curvature, components of the normal, etc.

We need an equation for the evolution of $\phi(\boldsymbol{x}, t)$, considering that the curve S is the level set given by:

$$S(t) = \{\boldsymbol{x} \in \mathbb{R}^2 | \phi(\boldsymbol{x}, t) = 0\}. \quad (3)$$

Let us take a point $\boldsymbol{x}(t), t \in \mathbb{R}^+$ of the deforming curve S. From its implicit definition given above we have:

$$\phi(\boldsymbol{x}(t), t) = 0. \quad (4)$$

Now, we can use the Chain Rule to compute the time derivative of this expression to get:

$$\phi_t + F|\nabla\phi| = 0, \quad (5)$$

where $F = \|dx/dt\|$ is called the speed function and ∇ is the gradient operator, with respect to $\boldsymbol{x}$. An initial condition $\phi(\boldsymbol{x}, t = 0)$ is required. A straightforward technique to define this function is to compute a signed-distance function as follows:

$$\phi(\boldsymbol{x}, t = 0) = \pm d, \qquad (6)$$

where d is the distance from $\boldsymbol{x}$ to the curve $S(\boldsymbol{x}, t = 0)$ and the sign indicates if the point is interior (+) or exterior (-) to the initial contour. The "fast marching method" (FMM) can be used to efficiently compute this function [12].

Finite difference schemes, based on uniform grids, can be used to solve equation (5). An entropy condition (once a grid node is burnt it stays burnt) is incorporated in order to drive the model to the desired solution.

In this higher dimensional formulation, topological changes can be efficiently implemented. Numerical schemes are stable (see section 5), and the model is general in the sense that the same formulation holds for 2D and 3D, as well as for merge and splits. Besides, geometric elements are easily computed. For example, the curvature (k) is given by:

$$k = \nabla \cdot \left(\frac{\nabla \phi}{||\nabla \phi||}\right) = \frac{\phi_y^2 \phi_{xx} - 2\phi_x \phi_y \phi_{xy} + \phi_{yy} \phi_x^2}{\left(\phi_x^2 + \phi_y^2\right)^{3/2}}, \qquad (7)$$

where the gradient (∇) and the divergent $(\nabla \cdot)$ are computed with respect to $\boldsymbol{x}$.

The update of the embedding function through expression (5) can be made cheaper if the narrow-band technique is applied. The key idea of this method comes from the observation that the curve can be moved by updating the level set function at a small set of points in the neighborhood of the zero set instead of updating it at all the points on the domain (see [11, 12] for details). Also, the governing equation (5) may be derived through a variational approach and the associated Euler-Lagrange expressions, as well shall see next for dual approaches.

4 Variational Formulation of Dual Models

For a given image $z: \Omega \subset \mathbb{R}^2 \to \mathbb{R}$, we consider an internal boundary Γ in the domain Ω that segments the image z into two subregions: foreground and background, represented by image intensities c_1 and c_2, respectively. We suppose that the target boundary Γ is limited by the curves Γ_1 and Γ_2 as shown in Figure 1. Hence, the Chan-Vese functional [18] computed for Γ_1 and Γ_2 gives:

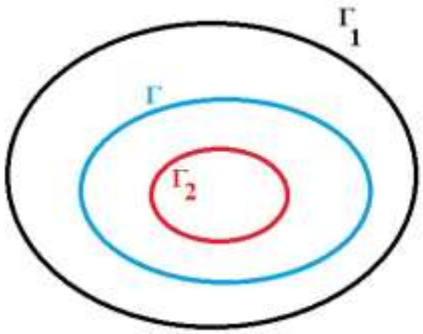

Figure 1: Outer (Γ_1) and inner (Γ_2) contours and the target boundary, denoted by Γ.

$$F(\Gamma_i, c_1, c_2) = \mu \int_{\Gamma_i} ds + \lambda_1 \int_{in(\Gamma_i)} |z(\boldsymbol{x}) - c_1|^2 \, d\boldsymbol{x} + \lambda_2 \int_{out(\Gamma_i)} |z(\boldsymbol{x}) - c_2|^2 \, d\boldsymbol{x}, \quad (8)$$

where in (Γ_i) means the region inside Γ_i and $out(\Gamma_i)$ the corresponding outside region of Γ_i, $i = 1,2$. Based on expressions (8) we could propose the following dual model:

$$D(\Gamma_1, \Gamma_2, c_1, c_2) = \frac{\mu}{2}\left(\int_{\Gamma_1} ds + \int_{\Gamma_2} ds\right)$$
$$+\lambda_1 \int_{in(\Gamma_1)} |z(\boldsymbol{x}) - c_1|^2 \, d\boldsymbol{x} + \lambda_2 \int_{out(\Gamma_2)} |z(\boldsymbol{x}) - c_2|^2 \, d\boldsymbol{x}. \quad (9)$$

So, we can seek for the desired curve Γ through the solution of the problem:

$$\min_{\Gamma_1, \Gamma_2} D(\Gamma_1, \Gamma_2, c_1, c_2). \quad (10)$$

To clarify this fact, we shall firstly notice that, given a generic curve $\overline{\Gamma}$, if $\Gamma_1 = \Gamma_2 = \overline{\Gamma}$ then $D(\overline{\Gamma}, \overline{\Gamma}, c_1, c_2) = F(\overline{\Gamma}, c_1, c_2)$. Moreover, D has a global minimum if $\overline{\Gamma} = \Gamma$, the target boundary in Figure 1. The procedure given by Algorithm 1 could solve this problem.

Algorithm 1 Procedure to Find Curve Γ

1: Initialization: Define curves $\Gamma_{1,0}, \Gamma_{2,0} \subset \Omega$.
2: **while** $\Gamma_{1,i} \neq \Gamma_{2,i}$ **do**
3: $\Gamma_{1,i+1} = \arg\min_{\Gamma} D\left(\Gamma, \Gamma_{2,i}, c_1, c_2\right)$
4: $\Gamma_{2,i+1} = \arg min_{\Gamma} D\left(\Gamma_{1,i}, \Gamma, c_1, c_2\right)$
5: $i \leftarrow i + 1$;
6: **end while**
7: Output: Solution Γ.

The general optimization Algorithm 1 is not a real procedure since there are some unspecified parts. For instance, the test $\Gamma_{1,i} \neq \Gamma_{2,i}$ can not be computationally performed due to numerical limitations. So, in practice, it should be replaced by a similarity test $sim(\Gamma_{1,i}, \Gamma_{2,i})$ where $sim(\Gamma_{1,i}, \Gamma_{2,i}) = 1$ if curves are close enough one each other and $sim(\Gamma_{1,i}, \Gamma_{2,i}) = 0$ otherwise [22, 17]. Moreover, a curve evolution algorithm based on some steepest descent methodology to minimize the functional D must control the topology of the solution in order to avoid self-intersections. Besides, and more fundamental for the optimization procedure, if $\Gamma_{1,i+1} = \Gamma_{1,i}, \Gamma_{2,i+1} = \Gamma_{2,i}$, and $\Gamma_{1,i+1} \neq \Gamma_{2,i+1}$ then Algorithm 1 enters an infinite loop.

Anyway, the Algorithm 1 keeps the main features of dual ACM models: one contour contracts from outside the target and another one expands from inside it (see video [42]). Such proposal makes possible to reduce the sensitivity to initialization through the comparison between the two contours positions, or some other similarity test.

To proceed with a more practical formulation, we follow the traditional level set development and introduce the Heaviside and its derivative (delta) function:

$$H_\varepsilon(x) = \frac{1}{2}\left(1 + \frac{2}{\pi}\arctan\left(\frac{x}{\varepsilon}\right)\right), \quad (11)$$

$$\delta_\varepsilon(x) \equiv \frac{dH_\varepsilon(x)}{dx} = \frac{\varepsilon}{\pi(\varepsilon^2 + x^2)}. \quad (12)$$

Figure 2 shows the behavior of $H_\varepsilon(\boldsymbol{x})$. If we replace $\boldsymbol{x} \leftarrow \boldsymbol{\phi}(\boldsymbol{x})$ in expression (12) we obtain:

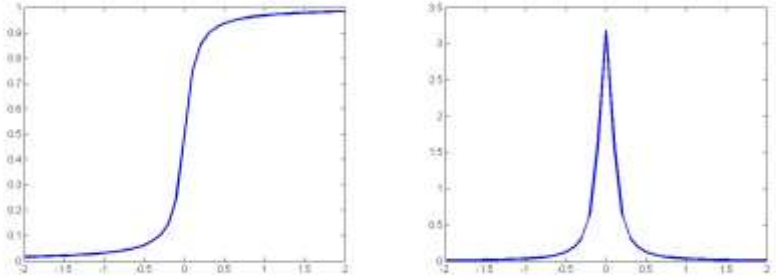

(a) (b)

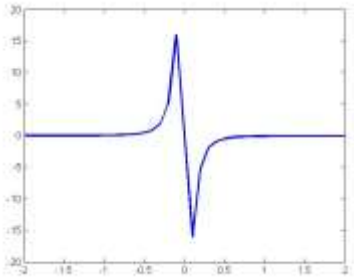

(c)

Figure 2: Heaviside function for $\varepsilon = 0.1$. (a) Function profile. (b) First derivative. (c) Profile of second derivative.

$$\delta_\varepsilon\big(\phi(\boldsymbol{x})\big) = \frac{\varepsilon}{\pi\left(\varepsilon^2+\left(\phi(\boldsymbol{x})\right)^2\right)}, \tag{13}$$

then:

$$\frac{\partial\delta_\varepsilon(\phi)}{\partial\phi} = -\frac{2\varepsilon}{\pi\left(\varepsilon^2+\left(\phi(\boldsymbol{x})\right)^2\right)^2} = -2\frac{\pi}{\varepsilon}\phi(\boldsymbol{x})\big(\delta_\varepsilon(\phi)\big)^2. \tag{14}$$

Now, we maintain the philosophy of dual models but the active contours will be implicitly represented using the level set formulation of section 3. So, the outer contour Γ_1 is given by the zero level set of an embedding function $\phi_1: \Omega \subset \mathbb{R}^2 \to \mathbb{R}$, while the inner contour Γ_2 is considered as the zero level set of another embedding function $\phi_2: \Omega \subset \mathbb{R}^2 \to \mathbb{R}$. We suppose that $\phi_1(\boldsymbol{x}) > 0$ if $\boldsymbol{x} \in in(\Gamma_1)$ and $\phi_1(\boldsymbol{x}) < 0$ if $\boldsymbol{x} \in out(\Gamma_1)$, with analogous construction for ϕ_2 and its zero level set Γ_2. Besides the curve length used in the functional (8), Chan-Vese also introduce the area of the region limited by the contour. However, the Chan-Vese model supposes that we can partition the image in almost homogeneous regions. In order to address this limitation in the dual formulation, we follow the LBF model proposed in [19] and make full use of the intensity information by replacing c_1 and c_2 to intensity functions $f_{i1}, f_{i2}: \Omega \subset \mathbb{R}^2 \to \mathbb{R}$, $i = 1,2$, to represent the gray values of the image z, inside (f_{i1}) and outside (f_{i2}) of the curve given by the zero-level set of ϕ_i. Moreover, we introduce the Gaussian kernel K_σ in order to control the scale to be considered [43]. Now, we will insert our presentation in a variational model based on Euler-Lagrange equations. In this way, we are going to build an energy functional:

$$E_i(\phi_i; f_{i1}, f_{i2}; \mu_{i1}, \mu_{i2}, \mu_{i3}, \mu_{i4}, \sigma) = \int_\Omega L_i(\phi_i; f_{i1}, f_{i2}; \mu_{i1}, \mu_{i2}, \mu_{i3}, \mu_{i4}, \sigma) d\boldsymbol{x}. \quad (15)$$

where L_i is the associated Lagrangian given as:

$$L_i(\phi_i; f_{i1}, f_{i2}; \mu_{i1}, \mu_{i2}, \mu_{i3}, \mu_{i4}, \sigma) = \mu_{i1}\delta_\varepsilon\big(\phi_i(\boldsymbol{x})\big)\|\nabla\phi_i(\boldsymbol{x})\| + \mu_{i2}H_\varepsilon\big(\phi_i(\boldsymbol{x})\big) + \mu_{i3}\int_\Omega K_\sigma(\boldsymbol{x},\boldsymbol{y})|z(\boldsymbol{y}) - f_{i1}(\boldsymbol{x})|^2 H_\varepsilon\big(\phi_i(\boldsymbol{y})\big)d\boldsymbol{y} + \mu_{i4}\int_\Omega K_\sigma(\boldsymbol{x},\boldsymbol{y})|z(\boldsymbol{y}) - f_{i2}(\boldsymbol{x})|^2 \Big(1 - H_\varepsilon\big(\phi_i(\boldsymbol{y})\big)\Big) d\boldsymbol{y}. \quad (16)$$

The first term in the right-hand side of Lagrangian (16) accounts for the arc length, the second term gives the area inside Γ_i, and the last two terms implements the LBF methodology [19]. We shall notice that, if we take expression (15) and set $f_{i1}(\boldsymbol{x}) = c_1$ and $f_{i2}(\boldsymbol{x}) = c_2$, in the limit $\sigma \longrightarrow 0$ (indicated as K_0 in the remaining text) we get the Chan-Vese level set formulation [18] of the energy functional (8). Also, we shall introduce a new symmetric term $\Theta = \Theta\big(H_\varepsilon(\phi_1), H_\varepsilon(\phi_2)\big)$ to model interaction between the level sets. So, we can put all these arrangements together and write a generalized level set version of the dual model (9) given by:

$$L = L_1(\phi_1; f_{11}, f_{12}; \mu_{11}, \mu_{12}, \mu_{13}, \mu_{14}, \sigma) + L_2(\phi_2; f_{21}, f_{22}; \mu_{21}, \mu_{22}, \mu_{23}, \mu_{24}, \sigma) + \tau\Theta\big(H_\varepsilon(\phi_1), H_\varepsilon(\phi_2)\big) \quad (17)$$

with the associated energy computed through the expression:

$$E = \int_\Omega L(\phi_1, \phi_2; \boldsymbol{f}; \boldsymbol{\mu}, \sigma, \tau) d\boldsymbol{x}, \quad (18)$$

where we summarize the arguments of L by assembling intensity functions in the array $\boldsymbol{f} = (f_{11}, f_{12}, f_{21}, f_{22})$ and the parameters in the vector $\boldsymbol{\mu} = (\mu_{11}, \mu_{12}, \mu_{13}, \mu_{14}, \mu_{21}, \mu_{22}, \mu_{23}, \mu_{24})$

Keeping f_{11}, f_{12}, ϕ_2 fixed and minimizing E with respect to the function ϕ_1 generates the Euler-Lagrange equation:

$$\frac{\partial L}{\partial \phi_1} - \frac{\partial}{\partial x}\left(\frac{\partial L}{\partial \phi_{1x}}\right) - \frac{\partial}{\partial y}\left(\frac{\partial L}{\partial \phi_{1y}}\right) = 0, \quad (19)$$

where $\phi_{1x} = \partial\phi_1/\partial x$ *and* $\phi_{1y} = \partial\phi_1/\partial y$. Expression (19) renders:

$$\mu_{12}\delta_\varepsilon(\phi_1) + \delta_\varepsilon(\phi_1)\big(\mu_{13}e(f_{11}) - \mu_{14}e(f_{12})\big)$$

$$-\mu_{11}\delta_\varepsilon(\phi_1(\boldsymbol{x}))\nabla.\left(\frac{\nabla\phi_1}{||\nabla\phi_1||}\right)+\tau\frac{\partial}{\partial\phi_1}\Theta\big(H_\varepsilon(\phi_1),H_\varepsilon(\phi_2)\big)=0, \quad (20)$$

where $\delta_\varepsilon(\phi_1)$ is computed by expression (13) and:

$$e(f_{1i})=\int_\Omega K_\sigma(x,y)|z(\boldsymbol{y})-f_{1i}(\boldsymbol{x})|^2\,d\boldsymbol{y},\ i=1,2. \quad (21)$$

To obtain expression (20) we use equation (17), and the fact that, from property (14), we can assume that $\partial\delta_\varepsilon(\phi)/\partial\phi\approx 0$ if $\phi(\boldsymbol{x})\approx 0$. We shall notice that, if we take expression (15) and set $f_{11}(\boldsymbol{x})=c_1$ and $f_{12}(\boldsymbol{x})=c_2$, and $\sigma=0$ then we get the Chan-Vese level set formulation [18] of the energy functional (8).

Now, keeping $\phi_1,\phi_2,f_{21},f_{22}$ fixed and minimizing E with respect to the function f_{11} and f_{12} by solving equations $\partial E/\partial f_{1i}=0$ gives:

$$f_{11}(\boldsymbol{x})=\frac{\int_\Omega K_\sigma(\boldsymbol{x},\boldsymbol{y})z(\boldsymbol{y})H_\varepsilon(\phi_1(\boldsymbol{y}))d\boldsymbol{y}}{\int_\Omega K_\sigma(\boldsymbol{x},\boldsymbol{y})H_\varepsilon(\phi_1(\boldsymbol{y}))d\boldsymbol{y}}, \quad (22)$$

$$f_{12}(\boldsymbol{x})=\frac{\int_\Omega K_\sigma(\boldsymbol{x},\boldsymbol{y})z(\boldsymbol{y})\big(1-H_\varepsilon(\phi_1(\boldsymbol{y}))\big)d\boldsymbol{y}}{\int_\Omega K_\sigma(\boldsymbol{x},\boldsymbol{y})\big(1-H_\varepsilon(\phi_1(\boldsymbol{y}))\big)d\boldsymbol{y}}. \quad (23)$$

Something analogous happens if we keep $\phi_1,f_{11},f_{12},f_{21},f_{22}$ fixed and minimizing E with respect to the function ϕ_2:

$$\frac{\partial L}{\partial\phi_2}-\frac{\partial}{\partial x}\left(\frac{\partial L}{\partial\phi_{2x}}\right)-\frac{\partial}{\partial y}\left(\frac{\partial L}{\partial\phi_{2y}}\right)=0, \quad (24)$$

generating the Euler-Lagrange equation:

$$\mu_{22}\delta_\varepsilon(\phi_2)+\delta_\varepsilon(\phi_2)\big(\mu_{23}e(f_{21})-\mu_{24}e(f_{22})\big)$$
$$-\mu_{21}\delta_\varepsilon(\phi_2(\boldsymbol{x}))\nabla.\left(\frac{\nabla\phi_2}{||\nabla\phi_2||}\right)+\tau\frac{\partial}{\partial\phi_2}\Theta\big(H_\varepsilon(\phi_1),H_\varepsilon(\phi_2)\big)=0, \quad (25)$$

where $e(f_{21})$ and $e(f_{22})$ are defined by expression (21) with f_{1i} replaced by f_{2i}. Like before, we can solve expressions $\partial E/\partial f_{2i}=0$ to minimize E with respect to the functions f_{21},f_{22} while keeping $f_{11},f_{12},\phi_1,\phi_2$ fixed to get:

$$f_{21}(\boldsymbol{x})=\frac{\int_\Omega K_\sigma(\boldsymbol{x},\boldsymbol{y})z(\boldsymbol{y})H_\varepsilon(\phi_2(\boldsymbol{y}))d\boldsymbol{y}}{\int_\Omega K_\sigma(\boldsymbol{x},\boldsymbol{y})H_\varepsilon(\phi_2(\boldsymbol{y}))d\boldsymbol{y}}, \quad (26)$$

$$f_{22}(\boldsymbol{x})=\frac{\int_\Omega K_\sigma(\boldsymbol{x},\boldsymbol{y})z(\boldsymbol{y})\big(1-H_\varepsilon(\phi_2(\boldsymbol{y}))\big)d\boldsymbol{y}}{\int_\Omega K_\sigma(\boldsymbol{x},\boldsymbol{y})\big(1-H_\varepsilon(\phi_2(\boldsymbol{y}))\big)d\boldsymbol{y}}. \quad (27)$$

The process of minimizing the functional given in (18) can be viewed from a dynamic point of view that unifies the description of shape and motion. In these models the embedding

functions are viewed as time-varying objects $\phi_1 = \phi_1(\boldsymbol{x}, t)$ and $\phi_2 = \phi_2(\boldsymbol{x}, t)$ and the solutions of the Euler-Lagrange equations becomes the stationary solution of expressions:

$$\frac{\partial \phi_i}{\partial t} = -\mu_{i2}\delta_\varepsilon(\phi_i) - \delta_\varepsilon(\phi_i)\big(\mu_{i3}e(f_{i1}) - \mu_{i4}e(f_{i2})\big)$$
$$+\mu_{i1}\delta_\varepsilon\big(\phi_i(\boldsymbol{x})\big)\nabla.\left(\frac{\nabla\phi_i}{||\nabla\phi_i||}\right) - \tau\frac{\partial}{\partial\phi_i}\Theta\big(H_\varepsilon(\phi_1), H_\varepsilon(\phi_2)\big),\ i = 1,2, \quad (28)$$

which are Hamilton-Jacobi equations, that must be constrained to boundary and initial conditions $\phi_{1,0} = \phi_1(\boldsymbol{x}, 0)$ and $\phi_{2,0} = \phi_2(\boldsymbol{x}, 0)$ (see section 5). Besides, it is straightforward to show that $E(\phi_1, \phi_2; \boldsymbol{f}; \boldsymbol{\mu}, \sigma, \tau) = E\big(\phi_2, \phi_1; \hat{\boldsymbol{f}}; \hat{\boldsymbol{\mu}}, \sigma, \tau\big)$, where $\hat{\boldsymbol{f}} = (f_{21}, f_{22}, f_{11}, f_{12})$ and $\hat{\boldsymbol{\mu}} = (\mu_{21}, \mu_{22}, \mu_{11}, \mu_{12}, \mu_{23}, \mu_{24}, \mu_{13}, \mu_{14})$ which we are going to use bellow to compact the pseudocode. Now, it is useful to rewrite the Algorithm 1 using the level set and variational formulation above. Before this, we shall write the right-hand side of equations (28) as $\mathbb{H}(\phi_1, \phi_2, f_{11}, f_{12}, \boldsymbol{\mu}, \sigma, \tau)$ and $\mathbb{H}(\phi_1, \phi_2, f_{21}, f_{22}, \boldsymbol{\mu}, \sigma, \tau)$, for $i = 1, 2$, respectively. Moreover, once the Algorithm 2 updates level set function $\phi_{1,i}$ to $\phi_{1,i+1}$ it is more efficient to use the latter when computing $\phi_{2,i+1}$.

Algorithm 2 Dual ACM Algorithm

1: Initialization: De ne curves $\Gamma_{1,0}$ and $\Gamma_{2,0}$
2: Build initial embedding functions: $\phi_{1,0}$ and $\phi_{2,0}$
3: Set parameters:$\mu = (\mu_{11}, \mu_{12}, \mu_{13}, \mu_{14}, \mu_{21}, \mu_{22}, \mu_{23}, \mu_{24}), \sigma, \tau$
4: $i = 0$;
5: **while** $\big(sim(\Gamma_{1,i}, \Gamma_{2,i}) = 0\big)$ **do**
6: $\quad \phi_{1,i+1} = \arg\min_{\phi_1} E\left(\phi_1, \phi_{2,i}; \boldsymbol{f}; \boldsymbol{\mu}, \sigma, \tau\right)$
7: $\quad \phi_{2,i+1} = \arg\min_{\phi_2} E\big(\phi_2, \phi_{1,i+1}; \hat{\boldsymbol{f}}; \hat{\boldsymbol{\mu}}, \sigma, \tau\big)$
8: $\quad i \leftarrow i + 1$;
9: $\quad$ Compute zero level sets $\Gamma_{1,i}$ and $\Gamma_{2,i}$
10: **end while**
11: Output: Solution Γ.

With Algorithm 2, we avoid self-intersections of the curves Γ_1 and Γ_2 once they are always zero level sets of the corresponding embedding functions. The zero level sets $\Gamma_{1,i}$ and $\Gamma_{2,i}$ in the line 9 of Algorithm 2 are compute through a 2D marching-cubes method [12]. However, we still need a similarity test to implement the

verification $\Gamma_{1,i} \neq \Gamma_{2,i}$. Moreover, and even more fundamental for dual approaches, if the energy E achieves a local minimum in the pair

Algorithm 3 PROCEDURE $\min_{\phi_1} E(\phi_1, \phi_2; \boldsymbol{f}; \boldsymbol{\mu}, \sigma, \tau)$

1: $\min_{\phi_1} E(\phi_1, \phi_2; \boldsymbol{f}; \boldsymbol{\mu}, \sigma, \tau)$
2: $j \leftarrow 0$;
3: Initialize ϕ_1 with its last update: $\phi_1(\boldsymbol{x}, 0) = \phi_{1,i}$;
4: **while** (;;) **do**
5: Compute f_{11} and f_{12} by setting $\phi_1(\boldsymbol{y}) \leftarrow \phi_1(\boldsymbol{y}, 0)$ in expressions (22)-(23)
6: Find stationary solution ϕ_1^* of expression:
7: $\frac{\partial \phi_1}{\partial t} = \mathbb{H}(\phi_1 \phi_2, f_{11}, f_{12}, \boldsymbol{\mu}, \sigma, \tau)$
8: subject to: $\phi_1(\boldsymbol{x}, 0) = \phi_{1,i}$,
9: set $\phi_{1,j+1} = \phi_1^*$
10: **if** $\left(sim\left(\Gamma_j, \Gamma_{j+1}\right) = 1\right)$ **then**
11: Return $\phi_{1,j+1}$
12: **else**
13: Reinitialize signed-distance function generating $\phi_{1,j+1}^*$,
14: $\phi_1(x, 0) = \phi_{1,j+1}^*$,
15: $j \leftarrow j + 1$,
16: **end if**
17: **end while**

$\left(\phi_{1,i}, \phi_{2,i}\right)$, then $\phi_{1,i+1} = \phi_{1,i}$ and both curves will remain at rest. Although Algorithm 2 can realize this fact by checking that $\Gamma_{1,i} \neq \Gamma_{2,i}$, it does not provide a way to go out this point. Before to enter mathematical details about dual approaches of the literature, and their solutions for the mentioned problems, we shall review numerical methods in this field.

5 Numerical Solution

Each equation given by expression (28) can be written in a general form:

$$G_t + \mathbb{H}\left(G, \frac{\partial G}{\partial x}, \frac{\partial G}{\partial y}, \frac{\partial^2 G}{\partial x^2}, \frac{\partial^2 G}{\partial y^2}, \frac{\partial^2 G}{\partial xy}, \boldsymbol{e}\right) = 0, \quad (29)$$

where $\mathbb{H}$ is, in general, a non-convex Hamiltonian, and $\boldsymbol{e} = \left(e(f_{11}), e(f_{12})\right)$ or $\boldsymbol{e} = \left(e(f_{21}), e(f_{22})\right)$, depending if we are working with equation (28) for $i = 1$ or $i = 2$, respectively. Therefore, following [12], we can use a first order numerical finite difference scheme, based on a regular discretization $\{(x_i, y_j), 1 \leq i \leq N, 1 \leq i \leq M\}$ of the image domain Ω, given by:

$$G_{i,j}^{n+1} = G_{i,j}^{n} - \Delta t \cdot \mathbb{H}\left(G_{ij}^{n}, \frac{D_{i,j}^{-x} + D_{i,j}^{+x}}{2}, \frac{D_{i,j}^{-y} + D_{i,j}^{+y}}{2}, \frac{D_{i,j}^{+x} - D_{i,j}^{-x}}{2\Delta x}, \frac{D_{i,j}^{+y} - D_{i,j}^{-y}}{2\Delta y}, D_{i,j}^{xy}, \boldsymbol{e}\right), \quad (30)$$

where $D_{i,j}^{-x}$ and $D_{i,j}^{+x}$ are first order finite-difference operators defined as:

$$D_{i,j}^{-x} G = \frac{G(x_i, y_j) - G(x_i - \Delta x, y_j)}{\Delta x}, \quad (31)$$

$$D_{i,j}^{+x} G = \frac{G(x_i + \Delta x, y_j) - G(x_i, y_j)}{\Delta x}, \quad (32)$$

following the same idea for $D_{i,j}^{-y}, D_{i,j}^{+y}$. In the case of $D_{i,j}^{xy} G$, that approximates the mix derivative in equation (30), we apply the scheme:

$$D_{i,j}^{xy} G = \frac{G(x_i + \Delta x, y_j + \Delta y) - G(x_i + \Delta x, y_j - \Delta y)}{4\Delta x \Delta y} + \frac{[-G(x_i - \Delta x, y_j + \Delta y) + G(x_i - \Delta x, y_j - \Delta y)]}{4\Delta x \Delta y}. \quad (33)$$

An initial condition $G(x, y, t = 0)$ is required to define $G_{i,j}^{0}$ in the numerical grid. A straightforward technique is to compute a signed-distance function given by expression (6). The boundary conditions could be implemented using Neumann boundary conditions [18]:

$$\frac{\delta_\varepsilon(G)}{\|\nabla G\|} \frac{\partial G}{\partial \boldsymbol{n}} = 0, \quad (34)$$

where $\boldsymbol{n}$ denotes the exterior normal to the boundary $\partial\Omega$, and $\partial G / \partial \boldsymbol{n}$ indicates the directional derivative of G respect to $\boldsymbol{n}$. Other possibility could be periodic boundary conditions: create an extra layer of ghost nodes around the domain whose values are direct copies of the G values along the actual boundaries. During the numerical simulation, at the end of each iteration, the new values on the boundary are copied to the ghost cells.

6 Variational Implicit Models

In this section, the image field is denoted by a function $z: \Omega \subset \mathbb{R}^2 \to \mathbb{R}$. The outer contour (Γ_1) is defined as the zero level set of an embedding function ϕ_1 and the inner contour (Γ_2) is the zero level set of another embedding function ϕ_2. We survey some dual level set models [23, 26, 31, 28, 27, 25], that are based on the variational approach established in section 4. Algorithm 2 is the basic one behind the focused techniques with the numerical scheme to solve the Hamilton-Jacobi equation in line 7 of Algorithm 3 given in section 5.

6.1 Dual Geometric Active Contour

The model proposed in [23] takes advantage of the Chan-Vese active contour technique [18] but introduces a term to model the interaction between the inner and outer contours to reduce the distance between them. Specifically, if we take the energy functional (18) and set $\boldsymbol{f} = (c_{11}, c_{12}, c_{21}, c_{22}) = \boldsymbol{cte}$, $\boldsymbol{\mu} = (\mu_{11}, 0, \mu_{13}, \mu_{14}, \mu_{21}, 0, \mu_{23}, \mu_{24},)$, $\sigma = 0$, and define the term that models the interaction between the curves as:

$$\Theta(\phi_1, \phi_2) = \left(H_\varepsilon\big(\phi_1(\boldsymbol{x})\big) - H_\varepsilon\big(\phi_2(\boldsymbol{x})\big)\right)^2, \qquad (35)$$

we get the energy functional proposed in [23]. In this case, we shall notice that expressions (21) becomes:

$$\mathrm{e}(c_{ij}) = \int_\Omega K_0(\boldsymbol{x}, \boldsymbol{y}) \left|z(\boldsymbol{y}) - c_{ij}\right|^2 d\boldsymbol{y} = \left|z(\boldsymbol{x}) - c_{ij}\right|^2,\ i, j = 1,2. \qquad (36)$$

The Hamilton-Jacobi equations associated to the Lagrangian (17) are:

$$\frac{\partial \phi_i}{\partial t} = \delta_\varepsilon(\phi_i)(\mu_{i3}|z(\boldsymbol{x}) - c_{i1}|^2 - \mu_{i4}|z(\boldsymbol{x}) - c_{i2}|^2) + \mu_{i1}\delta_\varepsilon(\phi_i)\nabla.\left(\frac{\nabla\phi_i(\boldsymbol{x})}{||\nabla\phi_i(\boldsymbol{x})||}\right)$$
$$+ (-1)^{i+1}\tau\delta_\varepsilon(\phi_i)\big[H_\varepsilon\big(\phi_1(\boldsymbol{x})\big) - H_\varepsilon\big(\phi_2(\boldsymbol{x})\big)\big], \qquad (37)$$

which define the evolution equations of the level set functions $\phi_i, i = 1,2$. The last term on the right-hand side of (37) is called the interaction term, which is defined to reduce the difference between the inner and outer contours. The minimization of dual level set energy (18) respect to c_{ij}, with parameters set as above, produces:

$$c_{i1} = \frac{\int_\Omega z(\boldsymbol{x}) H_\varepsilon(\phi_i(\boldsymbol{x}))d\boldsymbol{x}}{\int_\Omega H_\varepsilon(\phi_i(\boldsymbol{x}))d\boldsymbol{x}}, \quad i = 1,2, \qquad (38)$$

$$c_{i2} = \frac{\int_\Omega z(\boldsymbol{x})\big(1 - H_\varepsilon(\phi_i(\boldsymbol{x}))\big)d\boldsymbol{x}}{\int_\Omega\big(1 - H_\varepsilon(\phi_i(\boldsymbol{x}))\big)d\boldsymbol{x}}. \quad i = 1,2. \qquad (39)$$

The active contours can avoid local minima during the energy minimization because the last term in expression (37) forces the zero level sets Γ_1 and Γ_2 to get closer because $\Theta(\phi_1, \phi_2) = 0$ if and only if $\phi_1 = \phi_2$. The model is implemented using the Algorithm 2, with the numerical scheme of section 5.

In [23], this model is validated using $\varepsilon = 0.05$, $\mu_{11} = \mu_{21} = 0.005 \times 255^2$, $\mu_{13} = \mu_{23} = 1, \mu_{14} = \mu_{24} = 1, \tau = 2.5 \times 255^2$ in equations (37), and time step $\Delta t = 0.02$ in the numerical scheme of section 5. The computational experiments (page 2 of [23]) are executed with manual initialization of the dual ACM proposed, using two rectangles, one outside the target and another one inside the object (cup image). The obtained results outperform the Chan-Vese segmentation.

6.2 Dual Approach for HR-pQCT Segmentation

The segmentation of the bone in HR-pQCT (High Resolution peripheral Quantitative Computed Tomography) images remains a challenging task due to the image characteristics and the complex structures. In [26], the problem of separating the cortical bone from the background and the trabecular bone is addressed. The model is inspired in the work [38], where authors introduced localized energy ACMs that can segment heterogeneous objects using the local region information along the contour. Hence, based on [38], it is presented a dual deformable approach whose variational formulation uses a novel energy proposed to segment objects that share the same intensity level but with different textures. In [26] it is shown a typical example of the segmentation problem in this application. In this case, the region of interest is better represented by a ribbon that is bounded by two curves as pictured in Figure 3.

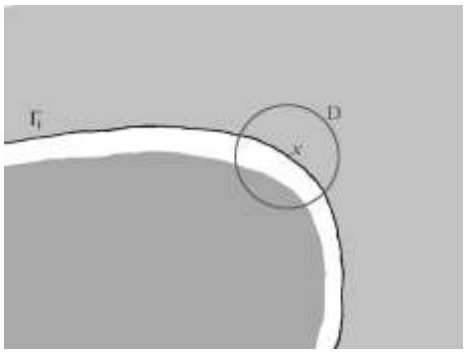

Figure 3: Neighborhood $D(\boldsymbol{x}, r)$ of each point $\boldsymbol{x}$ along the outer contour Γ_1 is split by the contour into $D(\boldsymbol{x}, r) \cap in(\Gamma_1)$ and $D(\boldsymbol{x}, r) \cap out(\Gamma_1)$.

The proposed approach moves the outer (Γ_1) and inner (Γ_2) contours toward the target region, reducing the local energy between them. This technique can be formulated by replacing $K_\sigma(\boldsymbol{x},\boldsymbol{y}) \leftarrow \delta_\varepsilon\big(\phi_1(\boldsymbol{x})\big)D(\boldsymbol{x},\boldsymbol{y})$ in the Lagrangian L_1 given by expressions (16), with $\mu_{12} = 0$, where $D(\boldsymbol{x},\cdot)$ represents the local neighborhood of the point $\boldsymbol{x}$ (Figure 3) as follows:

$$D(\boldsymbol{x},\boldsymbol{y}) = \begin{cases} 1, & if\ \big||\boldsymbol{x}-\boldsymbol{y}|\big| < r, \\ 0, & otherwise, \end{cases} \tag{40}$$

with r being the radius of the disk.

If we set $i = 1$ in expression (15) and minimize it respect to f_{11} and f_{12} we get:

$$f_{11}(\boldsymbol{x}) = \frac{\int_{\Omega_y} D(\boldsymbol{x},\boldsymbol{y})H_\varepsilon\big(\phi_1(\boldsymbol{y})\big)z(\boldsymbol{y})d\boldsymbol{y}}{\int_{\Omega_y} D(\boldsymbol{x},\boldsymbol{y})H_\varepsilon\big(\phi_1(\boldsymbol{y})\big)d\boldsymbol{y}}, \tag{41}$$

$$f_{12}(\boldsymbol{x}) = \frac{\int_{\Omega_y} D(\boldsymbol{x},\boldsymbol{y})\Big(1-H_\varepsilon\big(\phi_1(\boldsymbol{y})\big)\Big)z(\boldsymbol{y})d\boldsymbol{y}}{\int_{\Omega_y} D(\boldsymbol{x},\boldsymbol{y})\Big(1-H_\varepsilon\big(\phi_1(\boldsymbol{y})\big)\Big)d\boldsymbol{y}}, \tag{42}$$

which are the averages of pixels intensity inside (equation (41)) and outside (equation 42) the local neighborhood of point $\boldsymbol{x}$.

In the Lagrangian L_2 given by equation (16), we must replace $K_\sigma(\boldsymbol{x},\boldsymbol{y}) \leftarrow \delta_\varepsilon\big(\phi_2(\boldsymbol{x})\big)D(\boldsymbol{x},\boldsymbol{y})R(\boldsymbol{y})$, where R is a function developed to assure that only the points between the two curves are considered, and set $\mu_{22} = \mu_{23} = 0$. The function f_{22} is obtained by minimizing E_2 (energy (15)) with ϕ_2 remaining fixed:

$$f_{22}(\boldsymbol{x}) = \frac{\int_{\Omega_y} D(\boldsymbol{x},\boldsymbol{y})R(\boldsymbol{y})H_\varepsilon\big(\phi_2(\boldsymbol{y})\big)z(\boldsymbol{y})d\boldsymbol{y}}{\int_{\Omega_y} D(\boldsymbol{x},\boldsymbol{y})R(\boldsymbol{y})H_\varepsilon\big(\phi_2(\boldsymbol{y})\big)d\boldsymbol{y}}. \tag{43}$$

The regularization term for the inner contour is omitted because of the non-uniformity of the inner region (see page 2270 of in [26]). Besides, in the formulation [26], it is discarded the interaction term $\Theta\big(H_\varepsilon(\phi_1), H_\varepsilon(\phi_2)\big)$. The final energy functional of the dual contours is defined as:

$$E(\phi_1,\phi_2) = E_1(\phi_1) + \chi(\phi_1)\cdot E_2(\phi_2), \tag{44}$$

where χ is a function used to trig the second contour when the energy of contour Γ_1 is minimized, being defined as:

$$\chi(\phi_1^\star) = \begin{cases} 1, & if\ \phi_1^\star = \arg\min_{\phi_1} E_1\,, \\ 0, & otherwise. \end{cases} \tag{45}$$

By substituting the above equations into expression (28), with $\tau = 0$, the Hamilton-Jacobi equations for the method proposed in [26] are finally given by:

$$\frac{\partial \phi_1}{\partial t} = -\delta_\varepsilon(\phi_1)\big(\mu_{13}e(f_{11}) - \mu_{14}e(f_{12})\big) + \mu_{11}\delta_\varepsilon(\phi_1)\nabla.\left(\frac{\nabla\phi_1}{||\nabla\phi_1||}\right), \quad (46)$$

$$\frac{\partial \phi_2}{\partial t} = -\delta_\varepsilon(\phi_2)\mu_{24}e(f_{22}) + \mu_{21}\delta_\varepsilon(\phi_2)\nabla.\left(\frac{\nabla\phi_2}{||\nabla\phi_2||}\right), \quad (47)$$

where:

$$e(f_{1i}) = \int_\Omega \big[\delta\big(\phi(\boldsymbol{y})\big)D(\boldsymbol{x},\boldsymbol{y})\big]|z(\boldsymbol{y}) - f_{1i}(\boldsymbol{x})|^2\, d\boldsymbol{y}, \quad i = 1,2,$$

$$e(f_{22}) = \int_\Omega \big[\delta\big(\phi(\boldsymbol{y})\big)D(\boldsymbol{x},\boldsymbol{y})R(\boldsymbol{y})\big]|z(\boldsymbol{y}) - f_{22}(\boldsymbol{x})|^2\, d\boldsymbol{y},$$

and f_{1i} obtained by equations (41)-(42), and f_{22} computed using expression (43).

The dual model evolves according to Algorithm 2 to extract the boundaries of the desired object (represented by the ribbon in Figure 3). In this process, the outer curve is dedicated to the outer contour and it evolves through equation (46) to minimize the energy (44) with $\chi(\phi_1) = 0$. Then, the inner curve is triggered and starts evolving under the governing equations (47), to reduce the local energy between the two curves, computed through expression (44), with $\phi_1 = \phi_1^\star$, where $\phi_1^\star$ is the solution of Hamilton-Jacobi equation (46). These steps are repeated until the stopping criterion is achieved. The results shown in [26] were obtained with the above technique, with parameters $\mu_{11} = \mu_{13} = \mu_{14} = 1$ and $\mu_{21} = \mu_{24} = 1$, using a Heaviside function diferente from the previous section, given by:

$$H_\varepsilon(x) = \begin{cases} 0, & \text{if } x < -\varepsilon \\ 1, & \text{if } x > \varepsilon \\ \frac{1}{2}\left(1 + \frac{x}{\varepsilon} + \frac{1}{\pi}\sin\left(\pi\frac{x}{\varepsilon}\right)\right), & \text{otherwise.} \end{cases}$$

6.3 Segmentation of MR Diffusion Images

In [31], the variational dual level set formulation starts from a more general situation than the one considered in the previous sections, as shown in Figure 4. In this case, the zero level sets Γ_1 and Γ_2 divide the domain into four regions according to the signals of the embedding functions ϕ_1 and ϕ_2.

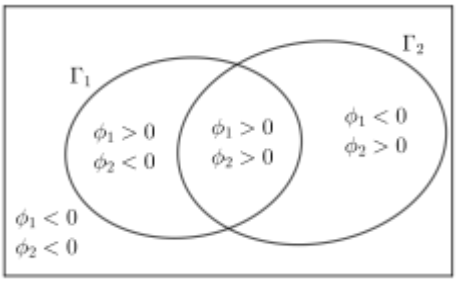

Figure 4 : Dual curves Γ_1 and Γ_2 in a generalized setup (adapted from [31]).

Besides, we shall notice that:

$$1 = \left[H_\varepsilon(\phi_1) + \left(1 - H_\varepsilon(\phi_1)\right)\right]\left[H_\varepsilon(\phi_2) + \left(1 - H_\varepsilon(\phi_2)\right)\right]$$

or

$$\begin{aligned} 1 = {} & H_\varepsilon(\phi_1)H_\varepsilon(\phi_2) + H_\varepsilon(\phi_1)\left(1 - H_\varepsilon(\phi_2)\right) + \\ & + \left(1 - H_\varepsilon(\phi_1)\right)H_\varepsilon(\phi_2) + \left(1 - H_\varepsilon(\phi_1)\right)\left(1 - H_\varepsilon(\phi_2)\right). \end{aligned} \quad (48)$$

Let us define: $H_{11} \equiv H_\varepsilon(\phi_1)H_\varepsilon(\phi_2), H_{12} \equiv H_\varepsilon(\phi_1)\left(1 - H_\varepsilon(\phi_2)\right), H_{21} \equiv H_\varepsilon(\phi_2)\left(1 - H_\varepsilon(\phi_1)\right)$, and $H_{22} \equiv \left(1 - H_\varepsilon(\phi_1)\right)\left(1 - H_\varepsilon(\phi_2)\right)$. Due to the properties of H_ε, it is easy to check that $0 \leq H_{ij} \leq 1$. So, this fact together with expression (48) show that the set of functions $\{H_{11}, H_{12}, H_{21}, H_{22}\}$ is a unity partition over the image domain Ω. Therefore, authors in [31] represent the segmented image as:

$$z(\boldsymbol{x}) = \sum_{i,j=1}^{2} c_{ij}\, H_{ij}(\boldsymbol{x}), \quad (49)$$

where c_{ij} are constant intensities, and they generalize the functional (15) in the form:

$$\tilde{E}_i = \int_\Omega \tilde{L}_i(\phi_i; \boldsymbol{c}; \boldsymbol{\mu}) d\boldsymbol{x}, \quad i = 1,2, \quad (50)$$

where $\boldsymbol{c} = (c_{11}, c_{12}, c_{21}, c_{22})$ is vector of mean intensities (see bellow), $\boldsymbol{\mu} = (\mu_{11}, \mu_{12}, \mu_{21}, \mu_{22})$ is a vector of parameters, and $\tilde{L}_i$ is given by:

$$\begin{aligned} \tilde{L}_i = {} & \mu_{i1}\delta_\varepsilon(\phi_i)\|\nabla\phi_i\| + \mu_{i2}H_\varepsilon(\phi_i) + \\ & + \mu_{i3}|z(\boldsymbol{x}) - c_{i1}|^2 H_{i1}(\boldsymbol{x}) + \mu_{i4}|z(\boldsymbol{x}) - c_{i2}|^2 H_{i2}(\boldsymbol{x}). \end{aligned} \quad (51)$$

If we keep fixed ϕ_1 and ϕ_2 and minimize functional $\tilde{E} = \tilde{E}_1 + \tilde{E}_2$ respect to c_{ij} we get:

$$c_{i1} = \frac{\int z(\boldsymbol{x}) H_{11}(\boldsymbol{x}) d\boldsymbol{x}}{\int H_{11}(\boldsymbol{x}) d\boldsymbol{x}}, \quad i = 1,2, \tag{52}$$

$$c_{i2} = \frac{\int z(\boldsymbol{x}) H_{12}(\boldsymbol{x}) d\boldsymbol{x}}{\int H_{12}(\boldsymbol{x}) d\boldsymbol{x}}, \quad i = 1,2. \tag{53}$$

If we consider the sets $\Omega_{ij} = \{\boldsymbol{x} \in \Omega; H_{ij}(\boldsymbol{x}) > 0\}$ we can notice that they form an (almost) disjoint partition of the image domain. Consequently, the average intensities c_{ij} computed by equations (52)-(53) include much less redundancy than in the case of the original Chan-Vese model. However, during level set evolution, we must be careful about the fact that some Ω_{ij} may vanish.

The governing equations are obtained by inserting the Lagrangian $\tilde{L} = \tilde{L}_1 + \tilde{L}_2$ into Euler-Lagrange equations (19) and (24), which renders:

$$\begin{aligned} \frac{\partial \phi_i}{\partial t} = {} & \mu_{i2}\delta_\varepsilon(\phi_i) - \mu_{i1}\delta_\varepsilon(\phi_i)\nabla.\left(\frac{\nabla\phi_i}{||\nabla\phi_i||}\right) \\ & +\delta_\varepsilon(\phi_i)[\,-\mu_{13}|z - c_{11}|^2 H_\varepsilon\left(\phi_{i+(-1)^{i+1}}\right) \\ & -\mu_{14}|z - c_{12}|^2\left(1 - H_\varepsilon\left(\phi_{i+(-1)^{i+1}}\right)\right) \\ & +\mu_{23}|z - c_{21}|^2 H_\varepsilon\left(\phi_{i+(-1)^{i+1}}\right) + \\ & +\mu_{24}|z - c_{22}|^2\left(1 - H_\varepsilon\left(\phi_{i+(-1)^{i+1}}\right)\right)] \end{aligned} \tag{54}$$

The segmentation algorithm used in [31] explores a combination of a greedy strategy with the Algorithm 2.

6.4 Dual Region-Scalable ACM

In [28, 27] it is proposed the dual active contour approach using the Lagrangian L, defined in expression (17), with parameters $\boldsymbol{\mu} = (\mu_{11}, 0, \mu_{13}, \mu_{14}, \mu_{21}, 0, \mu_{23}, \mu_{24})$. In this way, the following energy functional is proposed:

$$\begin{aligned} E = {} & \int_\Omega L(\phi_1, \phi_2; \boldsymbol{f}; \boldsymbol{\mu}, \sigma) d\boldsymbol{x} + \\ & +\varsigma\left(\int_\Omega \frac{1}{2}(\|\nabla\phi_1(\boldsymbol{x})\| - 1)^2 \, d\boldsymbol{x} + \int_\Omega \frac{1}{2}(\|\nabla\phi_2(\boldsymbol{x})\| - 1)^2 \, d\boldsymbol{x}\right) \\ & \tau \int_\Omega \left(H_\varepsilon\left(\phi_1(\boldsymbol{x})\right) - H_\varepsilon\left(\phi_2(\boldsymbol{x})\right)\right)^2 d\boldsymbol{x} \end{aligned} \tag{55}$$

where $\boldsymbol{f} = (f_{11}, f_{12}, f_{21}, f_{22})$, with $f_{i,j}$ computed according to expressions (22)-(23) and (26)-(27), being τ , ς weighting parameters.

The minimization of the functional (55) respect to ϕ_1 and ϕ_2, one at a time, gives Euler-Lagrange equations analogous to expressions (19) and (25), which generates the following governing equations:

$$\begin{aligned}\frac{\partial \phi_i}{\partial t} = &-\delta_\varepsilon(\phi_i)\big(\mu_{i3}e(f_{i1}) - \mu_{i4}e(f_{i2})\big) \\ &+\mu_{i1}\delta_\varepsilon(\phi_i)\nabla.\left(\frac{\nabla\phi_i}{\|\nabla\phi_i\|}\right) + \varsigma\left(\nabla^2\phi_i - \nabla.\left(\frac{\nabla\phi_i}{\|\nabla\phi_i\|}\right)\right) \\ &-2\tau(-1)^{i+1}\delta_\varepsilon(\phi_i)\big(H_\varepsilon(\phi_1) - H_\varepsilon(\phi_2)\big), \quad i = 1,2,\end{aligned} \tag{56}$$

where $e\big(f_{ij}\big)$ are given by expression (21).

In [27] it is described an application of the dual ACM defined by expression (56) for segmentation of transmission electron microscopy images of insulin granule cores [27]. The original image (page 419 of [27]) is processed using morphological operators in order to get the inner and outer contours. The evolution of these contours follow the Algorithm 2 and expression (56) for $i = 1,2$. The result is obtained by setting $\mu_{11} = \mu_{21} = 15.38 \times 255 \times 255$, $\mu_{13} = \mu_{23} = 1$, $\mu_{14} = \mu_{24} = 1$, and $\sigma = 7, \varsigma = 1$. The value of the numerical parameter is $\Delta t = 0.1$ and the Heaviside parameter is set to $\varepsilon = 1$.

6.5 Dual Models for Selective Segmentation

By selective segmentation we mean only segment a specific part among those objects that have the same feature. Such problem has been considered in [37], which proposes a selective segmentation model that uses a set of pre-defined points around the region of interest, as well as gradient information, to detect the boundary of the object of interest.

So, inspired in the works [37, 44, 45, 46, 47], it is proposed in [25] a dual level set technique that is based on LBF (expression (16)) and Chan-Vese [18] models simultaneously. One curve is used to find the segmentation of all boundaries and the other to focus on the selected target in order to fit the geometric constraints. In this model, the local and global region information are integrated, with the aim of dealing more efficiently with intensity inhomogeneity, weak edges and low contrast.

Let $S = \{\boldsymbol{x}_i \in \Omega; 1 \leq i \leq n\}$ be a set of n points nearby the real boundary of interest. Then, the model proposed in [37] is formulated through the energy functional:

$$E(\Gamma) = \int_\Gamma \hat{d}(\boldsymbol{x}) g(\|\nabla z(\boldsymbol{x})\|) ds, \tag{57}$$

where $\hat{d}: \Omega \longrightarrow \mathbb{R}$:

$$\hat{d}(\boldsymbol{x}) = \prod_{i=1}^{n}\left(1 - \exp\left[-\frac{\|\boldsymbol{x}-\boldsymbol{x_i}\|^2}{2\sigma^2}\right]\right), \tag{58}$$

and:

$$g(\|\nabla z(\boldsymbol{x})\|) = \frac{1}{1+\|\nabla z(\boldsymbol{x})\|^2}. \quad (59)$$

The key idea behind expression (57) is that the active contour stops the evolution nearby the points $\boldsymbol{x} \in \Omega$ with high gradient or that satisfies $\hat{d}(\boldsymbol{x}) \approx 0$. The place of such points gives a minimum for the functional (57).

The selective segmentation model (57) uses edge information. Therefore, if the image has fuzzy edges the evolving curve continues to move when achieves the boundary region which leads to fail. In order to improve the quality of segmentation, authors in [25] combine part of the Chan-Vese and LBF models to the selective segmentation approach (57) in a dual segmentation methodology: the inner curve evolves to locally segment the image and the other curve evolves to globally seek for objects of interest in the image. The proposed segmentation model, in the level set form, is defined as follows:

$$L = \mu_1 g(\|\nabla z\|)\delta_\varepsilon\big((\phi_1)\big)\|\nabla\phi_1(\boldsymbol{x})\| + \mu_2\hat{d}(\boldsymbol{x})g(\|\nabla z\|)\delta_\varepsilon\big((\phi_1)\big)\|\nabla\phi_1(\boldsymbol{x})\|$$
$$+\hat{L}\big(\phi_1,\phi_2;c_1,c_2,f_1,f_2;\lambda_1,\lambda_2,\lambda_3,\lambda_{1G},\lambda_{2G},\acute{\lambda_1},\acute{\lambda_2},\acute{\lambda_3},\acute{\lambda_{1G}},\acute{\lambda_{2G}},\omega,\sigma\big), \quad (60)$$

where:

$$\begin{aligned}\hat{L} = {} & \omega\left(\lambda_{2G}|z(\boldsymbol{x})-c_2|^2\left(1-H_\varepsilon\big(\phi_1(\boldsymbol{x})\big)\right)+\lambda_1|z(\boldsymbol{x})-c_1|^2H_\varepsilon\big(\phi_2(\boldsymbol{x})\big)\right)\\ & +\omega\left(\lambda_{1G}|z(\boldsymbol{x})-c_1|^2H_\varepsilon\big(\phi_1(\boldsymbol{x})\big)+\lambda_2|z(\boldsymbol{x})-c_1|^2H_{12}(\boldsymbol{x})\right)\\ & +\omega\big(\lambda_3|z(\boldsymbol{x})-c_2|^2H_{22}(\boldsymbol{x})\big)\\ & +(1-\omega)\acute{\lambda_{1G}}\int_\Omega K_\sigma|z(\boldsymbol{y})-f_1(\boldsymbol{x})|H_\varepsilon\big(\phi_1(\boldsymbol{x})\big)d\boldsymbol{y}\\ & +(1-\omega)\acute{\lambda_{2G}}\int_\Omega K_\sigma|z(\boldsymbol{y})-f_2(\boldsymbol{x})|^2\left(1-H_\varepsilon\big(\phi_1(\boldsymbol{x})\big)\right)d\boldsymbol{y}\\ & +(1-\omega)\acute{\lambda_1}\int_\Omega K_\sigma|z(\boldsymbol{y})-f_1(\boldsymbol{x})|^2H_\varepsilon\big(\phi_2(\boldsymbol{x})\big)d\boldsymbol{y}\\ & +(1-\omega)\acute{\lambda_2}\int_\Omega K_\sigma|z(\boldsymbol{y})-f_1(\boldsymbol{x})|^2H_{12}(\boldsymbol{y})d\boldsymbol{y}\\ & +(1-\omega)\acute{\lambda_3}\int_\Omega K_\sigma|z(\boldsymbol{y})-f_2(\boldsymbol{x})|^2H_{22}(\boldsymbol{y})d\boldsymbol{y}, \quad (61)\end{aligned}$$

where $H_{12} \equiv H_\varepsilon(\phi_1)\left(1-H_\varepsilon(\phi_2)\right)$ and $H_{22} \equiv \left(1-H_\varepsilon(\phi_1)\right)\left(1-H_\varepsilon(\phi_2)\right)$, like in section 6.3.

If we keep fixed ϕ_1, ϕ_2 and minimize functional (61) respect to c_1, c_2, f_1, and f_2 we get:

$$c_1 = \frac{\lambda_{1G}\int zH_\varepsilon(\phi_1)d\boldsymbol{x}+\lambda_1\int zH_\varepsilon(\phi_2)d\boldsymbol{x}+\lambda_2\int zH_{12}d\boldsymbol{x}}{\lambda_{1G}\int H(\phi_1)d\boldsymbol{x}+\lambda_1\int H(\phi_2)d\boldsymbol{x}+\lambda_2\int H_{12}d\boldsymbol{x}}, \quad (62)$$

$$c_2 = \frac{\lambda_{2G}\int z\big(1-H_\varepsilon(\phi_1)\big)d\boldsymbol{x}+\lambda_3\int zH_{22}d\boldsymbol{x}}{\lambda_{2G}\int\big(1-H_\varepsilon(\phi_1)\big)d\boldsymbol{x}+\lambda_3\int H_{22}d\boldsymbol{x}}, \quad (63)$$

$$f_1 = \frac{\lambda_{1G}' K_\sigma * (zH_\varepsilon(\phi_1)) + \lambda_1' K_\sigma * (zH_\varepsilon(\phi_2)) + \lambda_2' K_\sigma * (zH_{12})}{\lambda_{1G}' K_\sigma * H_\varepsilon(\phi_1) + \lambda_1' K_\sigma * H_\varepsilon(\phi_2) + \lambda_2' K_\sigma * H_{12}}, \quad (64)$$

$$f_2 = \frac{\lambda_{2G}' K_\sigma * \left(z(1 - H_\varepsilon(\phi_1))\right) + \lambda_3' K_\sigma * (zH_{22})}{\lambda_{2G}' K_\sigma * \left((1 - H_\varepsilon(\phi_1))\right) + \lambda_3' K_\sigma * H_{22}}. \quad (65)$$

The governing equations for ϕ_1 and ϕ_2 are obtained by inserting the Lagrangian L of expression (60) into equations (19) and (24), while keeping fixed c_1, c_2, f_1, f_2. The technique can be implemented through Algorithm 2, with the application of the additive operator splitting [48] to solve the Hamilton-Jacobi equations more efficiently.

In [25] it is presented a cell image segmentation result using the proposed technique (page 841 of [25]). It is used a manual initialization, composed by an outer circle and an inner contour, together with the geometric constraints defined by four fixed points to be used in expression (58).

In [29], it is presented a similar approach defined by the following Lagrangian:

$$\begin{aligned} L = {} & \frac{\mu_G}{2}(\|\nabla\phi_1(\boldsymbol{x})\| - 1) + \frac{\mu_L}{2}(\|\nabla\phi_2(\boldsymbol{x})\| - 1) + \mu_1 g(\|\nabla z\|)\delta_\varepsilon((\phi_1))\|\nabla\phi_1(\boldsymbol{x})\| \\ & + \mu_2 \hat{d}(x) g(\|\nabla z\|)\delta_\varepsilon((\phi_2))\|\nabla\phi_2(\boldsymbol{x})\| H_\varepsilon(\phi_1) \\ & + \hat{L}\left(\phi_1, \phi_2; c_1, c_2, c_1, c_2; \lambda_1, \lambda_2, \lambda_3, \lambda_{1G}, \lambda_{2G}, \lambda_1, \lambda_2, \lambda_3, \lambda_{1G}, \lambda_{2G}, \frac{1}{2}, 0\right). \end{aligned} \quad (66)$$

7 Non-Variational Dual Models

Likewise in the previous section, the image field is denoted by a function $z: \Omega \subset \mathbb{R}^2 \rightarrow \mathbb{R}$. In the first and second models, presented in [30, 32], the outer contour (Γ_1) is defined as the zero level set of an embedding function ϕ_1 and the inner contour (Γ_2) is the zero level set of another embedding function ϕ_2. In the third model, both inner and outer contours are zero level sets of the same embedding function [6]. However, in these cases, each level set function is governed by an equation (like (5)) that is not explicitly derived from Euler-Lagrange expressions.

7.1 Coupled Level Set Method

In [30] authors describe a method for bladder wall segmentation in magnetic resonance imaging (MRI) that works using T2- and T1-weighted MRI images [49]. Some image samples are pictured in [30] to help the visualization of the segmentation problem in both T2-weighted and T1-weighted axial images. A new coupling technique for level sets is formulated and tested on 54 T2- and T1-weighted image pairs.

The commonly used gradient based edge function, given by expression (59) is sensitive to noise, image inhomogeneities, and blurring. Therefore, it is not a good

feature indicator for MRI images which has forced the development of more sophisticated pre-processing stages. So, based on [50] it is used in [30] the wavelet transform to provide a way to describe both frequency and spatial information contained in the image. Wavelets give the basis for a multiresolution theory that incorporates techniques from subband coding and filter banks in signal analysis [51]. An interesting characteristic of wavelets is that their application results in a reduction of the amount of data by a factor of two, while preserving the main features on their coefficients of approximation. The obtained coefficients can be used to compute new feature fields $FA : \Omega \longrightarrow \mathbb{R}$, more appropriate for edge function definition in the form:

$$g_{FA}(\boldsymbol{x}) = \frac{1}{1+\alpha \cdot FA(\boldsymbol{x})}, \quad (67)$$

where α is a parameter that controls the slope of the function g_{FA} (see [50] for details).

In the proposed methodology, ϕ_2 is obtained from the segmentation in T2 image using the geodesic active contours model [40], equipped with the edge function in expression (67). Then, it is fixed and two techniques, named switch and spring methods are tested to segment the outer wall in the T1 image. In the former, ϕ_1 evolves under the governing equation:

$$\frac{\partial \phi_1}{\partial t} = \left(\gamma \nabla \cdot \left(g_{FA}(I_{T_1}) \frac{\nabla \phi_1}{\|\nabla \phi_1\|}\right) + \left(1 - H_\varepsilon(\phi_2 - d)\right) c g_{FA}(I_{T_1})\right) \|\nabla \phi_1\|, \quad (68)$$

where g_{FA} is given above. The factor $\left(1 - H_\varepsilon(\phi_2 - d)\right)$ is the stopping criterion of a balloon (inflation) force as H_ε is the Heaviside function (equation (11)) and d is the maximum distance allowed for the balloon force to act away from the inner wall boundary Γ_2. The parameter $\gamma \in \mathbb{R}$ is the contour coefficient and $c \in \mathbb{R}$ controls the magnitude of the balloon force. For the spring method, the evolution is formulated as:

$$\frac{\partial \phi_1}{\partial t} = \left(\gamma \nabla \cdot \left(g_{FA}(I_{T_1}) \frac{\nabla \phi_1}{\|\nabla \phi_1\|}\right) + c g_{FA}(I_{T_1}) - k\phi_2\right) \|\nabla \phi_1\|, \quad (69)$$

where γ and c are real constants as before. The function ϕ_2 is initialized as a signed distance function, like in expression (6). Therefore, the value $\phi_2(x, y)$ represents the shortest distance from the point (x, y) to the inner wall contour Γ_2. Hence, the term $k\phi_2$ in expression (69) can be thought of as a spring force that acts in between the inner and outer contours. Consequently, the parameter k corresponds to the spring constant.

7.2 Segmentation of Pulmonary Nodules

The model presented in [32] can be implemented using energies E_1 and E_2 for the curves Γ_1 and Γ_2, given by:

$$E_i = \int_\Omega L_i(\phi_i; c_{i1}, c_{i2}; \mu_{i1}, \mu_{i2}, \mu_{i3}, \mu_{i4}, 0)d\boldsymbol{x}, \quad i = 1,2, \qquad (70)$$

where L_i is defined by expression (16). The novelty of the methodology is the parametrization of the model which is performed using the pixel correlation (PC) that is defined by:

$$PC_i = r\frac{z_{max}^{in,i} - z_{min}^{in,i}}{z_{max}} + \frac{2(1-r)}{N_a^i z_{max}}\int_\Omega |z(\boldsymbol{x}) - c_{i1}|^2 H_\varepsilon(\phi_i)d\boldsymbol{x}, \qquad (71)$$

where $i = 1,2$, z_{max} is the maximum gray scale intensity in Ω, $z_{max}^{in,i}$ and $z_{min}^{in,i}$ are maximum and minimum gray scale intensities inside the curve Γ_i, N_i^a is the number of pixels of $in(\Gamma_i)$, and $r \in [0,1]$. So, in [32] the parameters of the expression (70) are computed by:

$$\mu_{i1} = k \cdot PC_i, \qquad (72)$$

$$\mu_{i2} = k \cdot (1 - PC_i), \qquad (73)$$

$$\mu_{i3} = (1 - k) \cdot PC_i, \qquad (74)$$

$$\mu_{i4} = (1 - k) \cdot (1 - PC_i), \qquad (75)$$

with $k \in [0,1]$, and $i = 1,2$. In this technique wavelet coefficients are used to compute the energies of different regions of the image signal and the inner/outer contours are defined by thresholding these fields. The governing equations of the level set functions ϕ_1 and ϕ_2 are given by expression (28) with $\sigma = \tau = 0$ and the other parameters computed according to equations (72)-(75). The dual evolution follows a procedure analogous to Algorithm 2, but in this case the energies (70) are calculated and one level set with maximum energy is selected to evolve based on the corresponding governing equation. When it stops moving, the energies are re-computed and compared to evolve the one with larger energy. This process continues until one level set superposes the other according to the similarity test. We shall highlight the fact that the expressions (20)-(25) are not the Euler-Lagrange equations associated with the functional (18) if the parameters are computed as above. That is why we consider this technique as a non-variational dual model in this review.

7.3 Dual-Level-Set Approach

Differently from all the techniques described in the previous sections, the Dual-Level-Set approach presented in [6] formulates the dual active contour model using only one embedding function. To set ideas, let us consider the Figure 5.(b), which shows two contours bounding the search space and Figure 5.(a) that pictures a

surface which zero level set is the union of the two contours just presented. Like before, the target boundary Γ belongs to the region bounded by the level set contours.

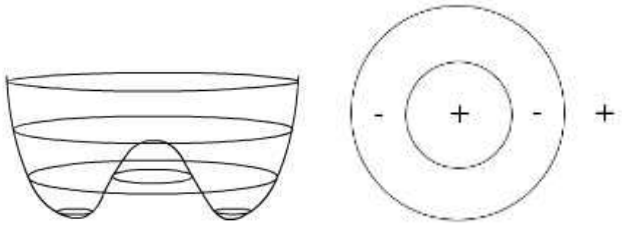

(a) (b)

Figure 5: (a) Embedding function for Dual-Level-Set approach. (b) Zero level sets and corresponding embedding function signals (source [22]).

If the surface pictured in Figure 5.(a) evolves such that the two level set curves in Figure 5.(b) get closer, we can apply an analogous of Algorithm 2 to perform the segmentation. That is the key idea of the method proposed by some of us in [6]. Likewise in the previous sections, the proximity of the dual active contours gives a stopping criterion. However, in this case, both contours are level sets of the same embedding function. In this context, the Dual-Level-Set approach presented in [6] is based on the following level set model:

$$\phi_t = -F\|\nabla\phi\| + \varepsilon\nabla^2\phi + \beta\nabla P \cdot \nabla\phi, \qquad (76)$$

where:

$$F = -\frac{1+\alpha k}{1+\|\nabla z\|^2}, \qquad (77)$$

with α, β being scale parameters, $P = -\|\nabla z\|^2$, and k is the curvature calculated by expression (7).

The evolution of the inner and outer contours follows this governing equation and are interdependent due to the embedding function. However, once the evolution stops, we must evaluate the similarity between the two contours and apply an extra term, named driving velocity in [6], to go out local minima. The numerical scheme is the one summarized in section 5 with the derivatives computed according to numerical approximations in expressions (31)-(33). The initialization and boundary conditions are given by equations (6) and (34).

As usual in some level set approaches [52], it is used in [6] the narrow band method; that is, only the values of ϕ within a tube placed around each ACM are updated. When the zero level set moves

near to the edge of the tube boundary, the computation is stopped and a new tube is built with the zero level set at the center. For Dual-Level-Set approach, the narrow band is attractive not only for computational aspects but also because it allows an efficient way to evaluate similarity between two contours. In fact, the Dual-Level-Set takes the procedure pictured in Figure 6: firstly, the intersection point is computed (Figure 6.(a)); then, a neighborhood of this point (Figure 6.b) is taken and the algorithm stops to update the function ϕ in all the grid points inside it or the speed function for these points is set to zero. In [6], authors said that those grid points are frozen ones.

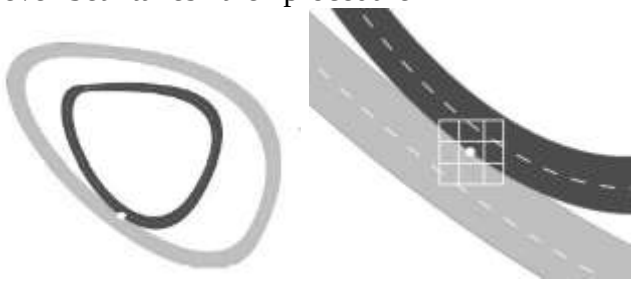

(a) (b)

Figure 6: (a) Narrow bands touching each other. (b) Neighborhood to define similarity between contours. (source [22])

Once the curves stop moving, it is necessary to decide in which grid points to add a driving velocity. It is an extra velocity term which goal is to keep contours moving again. In this way, a less sensitive model to the initial position of the deformable contours is obtained. To accomplish this task the Dual-Level-Set technique adds an extra velocity term to equation (76), called V_{driv}.

We must be careful when choosing the grid points to apply this term. The contours may be nearby the boundary somewhere, but far away from the target in another place. We should automatically realize this fact when they stop moving. To accomplish this, we can use the affinity operator. Based on this operator, we can define an affinity function that assigns to a grid point inside the narrow band a $0-1$ value: 0 for the grid points most likely to lie away from the target boundaries and 1 otherwise. Such affinity operator can be defined through fuzzy segmentation methods [53], image transforms [54], region statistics [55], etc. The whole Dual-Level-Set algorithm can be summarized as follows: (1) Initialization through step functions; (2) Evolution until curves stop. (3) Evaluate similarity. If frozen, stop. (4) Add V_{drive} for some time steps. (5) After that, turn-off V_{drive}. Go to step 2. When all the grid points inside the narrow bands are frozen, the Dual-Level-Set evolution stops and apply a search based algorithm (like Viterbi [56]) to get the final result.

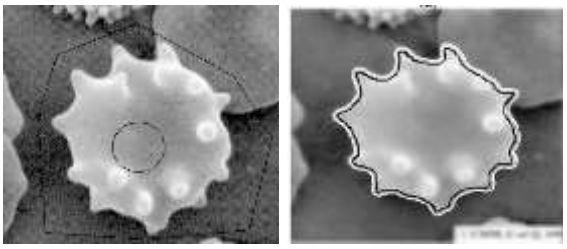

(a) (b)

Figure 7: (a) Original image and Dual-Level-Set initialization. (b) Result obtained using Dual-Level-Set. (source [22])

Figure 7 shows the application of the Dual-Level-Set to segment the cell image of Figure 7.(a), that pictures the outer curve and the inner one, placed by the user. The Dual-Level-Set parameters are: $\alpha = 0.1, \varepsilon = 2.0, \beta = 0.1$, and $\Delta t = 0.05$. The Dual-Level-Set result is shown in Figure 7.b.

8 Discussion

An important point for dual level set models is how to proceed the evolution after both deformable curves come at rest but are far from each other, as pictured in Figure 8.(a). Expression (35) is used to reduce the distance between the zero level sets. However, it does not take into account image features in order to avoid that portions of the zero level sets pass over the desired boundary. The LBF model (equation (21)), its variants in expressions (41)-(42), and the Chan-Vese proposal (equation (36)), try to address this issue by incorporating region features in the Euler-Lagrange force balance. However, such balance depends on parameter settings which is not a trivial task for ACM models. In general, the most commonly used method to set parameters is trial and error. You repeatedly modify the parameters and evaluate the result. Few works have been done to calibrate parameters automatically in ACM models [57]. This point is critical for dual level sets as we have both the outer and inner governing equations to calibrate.

The affinity operator applied by the Dual-Level-Set [6] is used to automatically determine the portions of each deformable curve that most likely are far away from the target. The selective segmentation, presented in section 6.5, is another alternative in this line, because the energy (57) goes to zero nearby the set S of selected points.

The policy used in section 7.2 to re-compute the energies associated to the zero level sets is important to choose, among the functions ϕ_1 and ϕ_2, which one will be evolved. The Algorithm 2, which implements most of the revised dual ACMs, should incorporate such energy balance in further versions.

Dual level set models are topologically adaptable deformable techniques, which increases their range of applications. However, such generality increases the search space complexity and the chances to get trap in local minima. So, the utilization of selective segmentation approaches (section 6.5) is too important if we want to explore the topological capabilities of dual level sets.

Also, the similarity operator used as a stopping criterion in Algorithm 2 has limitations when the boundary is represented by a ribbon. Consequently, its precision may be not enough to allow a superposition between the zero level sets. In such cases, illustrated in Figure 8.(b), it is more efficient to apply dual models just to reduce the search space and then, to apply a search based technique to get the final result (Figure 8.(c)), like performed in parametric dual snakes [17]. This procedure is attractive because it simplifies the choice of parameters for the dual method and makes lower the computational cost of the application of a global optimization technique (see [17] for details).

Despite of the capabilities to reject local minima, dual models have also some disadvantages. Firstly, the method is at least two times more expensive than single approaches. Secondly, the initialization may be a tedious task because the user should set two curves at the beginning of the process. As already mentioned, the setup of parameters is also another point to be careful because in this case there are two snakes to be set. The technique presented in section 7.2 addresses the initialization and choice of parameters by thresholding wavelet based energy fields computed over the image intensities and by computing expressions (72)-(75), respectively.

To compare the Dual-Level-Set and the dual geometric active contour [6, 23], we must firstly notice that the latter uses two different level set functions to represent dual contours which increases the flexibility to represent inner/outer curves if compared with the former that applies only one level set function. To see this, for simplicity, we consider the one dimensional version of the segmentation problem. In this case, a simplified level set equation can be written as [52]:

$$\phi_t + \frac{\partial \phi}{\partial x} F = 0. \qquad (78)$$

The main point is to design the speed function F such that $\phi_t > 0$. If we set the sign of F opposite to the one of ϕ_x we get this goal, once:

$$\phi_t = -\frac{\partial \phi}{\partial x} F. \qquad (79)$$

Hence, considering the embedding function profile of Figure 5, the desired behavior can be obtained by the sign distribution of F, shown in Figure 9.

However, we should notice that $\phi_x = 0$ for singular points. So, the values of ϕ remain constant over these points because ϕ_t becomes null. Thus, we should be

careful about the surface evolution nearby the singular points because anomalies

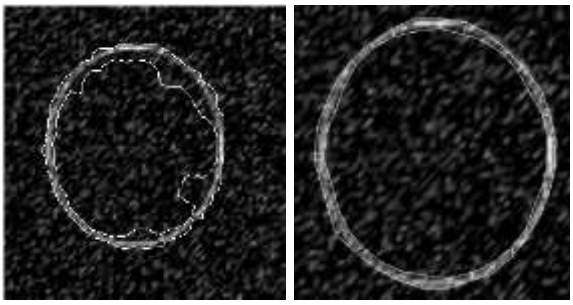

(a) (b)

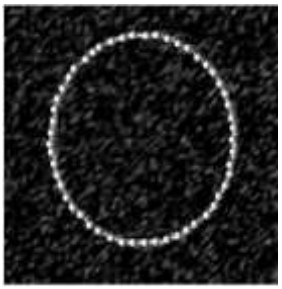

(c)

Figure 8: (a) Dual ACM before the segmentation is completed. (c) Search space defined by dual deformable models. (c) Final result obtained by a search based method (source [58]).

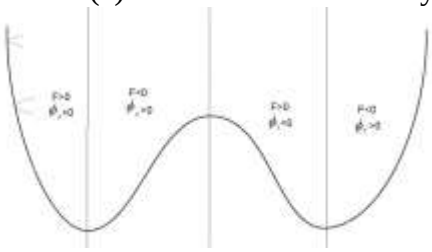

Figure 9: Speed function against level set function signals (source [22]).

may happen. The introduction of the Laplacian (viscosity) term in expression (76) aims to address this issue. However, the governing equation (76) updates both the zero level sets once they are implicitly represented by the same level set function ϕ. Such feature makes the control of the segmentation process sensitive to parameters choice and numerical issues.

As future works in dual ACM models based on level set methods we can list the following tasks.

- The combination of shape models with level sets [59] could generate dual approaches less sensitive to parameter choice because each deformable model will evolve constrained to the shape space of the target. However, such solution limits also the application of the method for general topologies.
- A fundamental and more difficult point for Dual ACM models is how to proceed the evolution after both active contours come at rest but they are far from each other. The level set with higher energy must be evolved, but the method should automatically realize the level set regions most likely to lie away from the target boundary. The affinity operator (section 7.3) is a methodology to address this problem but its implementation depends on elements that are application dependent, which opens new research possibilities for image transforms (like wavelets) or even machine learning techniques to improve the capability to decide how to go away from a local minimum.
- User interaction: The user can interfere in the dual level set model in the initialization, to define the inner/outer contours or to specify a set of points around the boundary of interest, like performed in section 6.5. Specific graphical interfaces must be designed with this aim in order to make these tasks as user-friendly as possible.
- Comparison between dual level set performances: in this survey we have focused in theoretical aspects, trying to put dual level set models in a common mathematical background. The next step is to compare the efficiency and computational performance of these algorithms.
- When deriving the Euler-Lagrange equations (20) and (25), we shall notice that the following term was not considered:

$$\frac{\partial \delta_\varepsilon(\phi)}{\partial \phi}\left|\left|\nabla\phi\right|\right| = \left(-2\frac{\pi}{\varepsilon}\phi\left(\delta_\varepsilon(\phi)\right)^2\right)\left\|\nabla\phi\right\|. \qquad (80)$$

Due to expression (14), nearby the zero level set $(\phi(\boldsymbol{x}) \approx 0)$, we have:

$$\frac{\partial \delta_\varepsilon(\phi)}{\partial \phi} \approx 0.$$

However, Figure 2.(c) shows that this term may be not negligible. Therefore, we shall analyze the influence of expression (80) in the governing equations (28).

9 Conclusions and Final Remarks

Dual approaches are powerful techniques to address the sensitivity to local minima of usual ACM models. The idea of using two snakes to seek for the global minimum, originally proposed in [20], has been explored through level set along the literature. Since the initial works [6, 23], dual ACM models based on level set techniques have been proposed for segmentation of medical and biological images, as reported in this survey.

The idea of embedding the original dual ACM technique in topologically adaptable approaches started in the parametric ACM scenario [60]. The class of dual level set approaches introduces another degree of freedom in such methodology by using embedding functions. In this paper, we report important techniques in that ACM category, starting from variational formulations and covering also non-variational implicit techniques. Advantages and drawbacks of dual ACM models based on level set methods are also discussed with some future works pointed out. Among the application fields, we believe that cell image segmentation is a promising one due to the kind of structures and object topologies therein.

References

[1] T. M. Lehmann, H. P. Meinzer, and Thomas Tolxdorff. Advances in biomedical image analysis–past, present and future challenges. *Methods of information in medicine*, 43 4:308–14, 2004.

[2] Alper Yilmaz, Omar Javed, and Mubarak Shah. Object tracking: A survey. *ACM Comput. Surv.*, 38(4), December 2006.

[3] J. S. Cardoso and L. Corte-Real. Toward a generic evaluation of image segmentation. *IEEE Transactions on Image Processing*, 14(11):1773–1782, Nov 2005.

[4] Bharath Sathya and R.Manavalan. Image segmentation by clustering methods: Performance analysis. *International Journal of Computer Applications*, 29(11), September 2011.

[5] M. Kass, A. Witkin, and D. Terzopoulos. Snakes: Active contour models. *International Journal of Computer Vision*, 1(4):321–331, 1988.

[6] Gilson A. Giraldi, Paulo Rodrigues, Jasjit Suri, Rodrigo L. S. Silva, and Antonio L. Apolinário Jr. Level set formulation for dual snake models. In Jasjit Suri and Aly Farag (Editors), editors, *Deformable models: clinical and biological applications*. Springer, NY, 2006.

[7] Amar Mitiche and Ismail Ben Ayed. *Variational and Level Set Methods in Image Segmentation*. World Scientific Publishing, 2010.

[8] J. Montagnat, H. Delingette, and N. Ayache. A review of deformable surfaces: topology, geometry and deformation. *Image and Vision Computing*, 19(14):1023 – 1040, 2001.

[9] Zohreh Azimifar and Mahsa Mohaddesi. Active surface model improvement by energy function optimization for 3d

segmentation. *Computers in Biology and Medicine*, 59:87 – 97, 2015.

[10] Sambhunath Biswas and Brian C. Lovell. *Bezier and splines in image processing and machine vision*. Springer-Verlag, 2008.

[11] R. Malladi, J. A. Sethian, and B. C. Vemuri. Shape modeling with front propagation: A level set approach. *IEEE Trans. Pattern Anal. Mach. Intell.*, 17(2):158–175, 1995.

[12] J. A. Sethian. *Level Set Methods: Evolving Interfaces in Geometry, Fluid Mechanics, Computer Vision and Materials Sciences*. Cambridge University Press, 1996, 1996.

[13] Dimitris N. Metaxas. *Physics-Based Deformable Models: Applications to Computer Vision, Graphics, and Medical Imaging*. Kluwer Academic Publishers, Norwell, MA, USA, 1st edition, 1996.

[14] Jasjit S. Suri and Aly Farag. *Deformable Models V. 1&2*. Springer Publishing Company, Incorporated, 1st edition, 2007.

[15] Daniel Cremers, Mikaël Rousson, and Rachid Deriche. A review of statistical approaches to level set segmentation: Integrating color, texture, motion and shape. *International Journal of Computer Vision*, 72:195–215, 2006.

[16] T. McInerney and D. Terzopoulos. Topology adaptive deformable surfaces for medical image volume segmentation. *IEEE Trans. on Medical Imaging*, 18(10):840–850, October 1999.

[17] Gilson A. Giraldi, Edilberto Strauss, and Antonio A. F. Oliveira. Dual-t-snakes model for medical imaging segmentation. *Pattern Recognition Letters*, 24:993–1003, 2003.

[18] Tony F. Chan and Luminita A. Vese. Active contours without edges. *IEEE transactions on image processing: a publication of the IEEE Signal Processing Society*, 10 2:266–77, 2001.

[19] Chunming Li, Chiu-Yen Kao, John C. Gore, and Zhaohua Ding. Implicit active contours driven by local binary fitting energy. *2007 IEEE Conference on Computer Vision and Pattern Recognition*, pages 1–7, 2007.

[20] Steve R. Gunn and Mark S. Nixon. A robust snake implementation; a dual active contour. *IEEE Trans. Pattern Anal. Mach. Intell.*, 19:63–68, 1997.

[21] Chung-Ming Chen, H. H. Lu, and Annie Hsiao. A dual-snake model of high penetrability for ultrasound image boundary extraction. *Ultrasound in medicine & biology*, 27 12:1651–65, 2001.

[22] Gilson A. Giraldi, Paulo Rodrigues, Jasjit Suri, and Sameer Singh. Dual Active Contour Models for Medical Image Segmentation. In *Image Segmentation*. Intech Open Access Pubisher, 2012.

[23] Changhong Wang Guopu Zhu, Qingshuang Zeng. Dual geometric active contour for image segmentation. *Optical Engineering*, 45:45 – 45 – 3, 2006.

[24] Huafeng Wang, Lihong C. Li, Xinzhou Wei, Wanquan Liu, Yuehai Wang, and Zhengrong Liang. A new framework for detection of initial flat polyp candidates based on a dual level set competition model. In *Medical Imaging: Computer-Aided Diagnosis*, 2017.

[25] Wang Xueqin, Li Shurong, Li Jiaojiao, Wang Jiayan, and Zhang Minyi. A novel segmentation model with dual level set function based on chan-vese and local binary fitting models. *2016 3rd International Conference on Systems and Informatics (ICSAI)*, pages 837–842, 2016.

[26] Mohamed Hafri, Rachid Jennane, Eric Lespessailles, and Hechmi Toumi. Dual active contours model for hr-pqct cortical bone segmentation. *2016 23rd International Conference on Pattern Recognition (ICPR)*, pages 2270– 2275, 2016.

[27] David Nam, Judith Mantell, David R. Bull, Paul Verkade, and Alin Achim. A novel framework for segmentation of secretory granules in electron micrographs. *Medical image analysis*, 18 2:411–24, 2014.

[28] D. Nam, J. Mantell, D. Bull, P. Verkade, and A. Achim. Active contour based segmentation for insulin granule cores in electron micrographs of beta islet cells. In *2012 Annual International Conference of the IEEE Engineering in Medicine and Biology Society*, pages 5339–5342, Aug 2012.

[29] Lavdie Rada and Ke Chen. A variational model and its numerical solution for local, selective and automatic segmentation. *Numerical Algorithms*, 66:399–430, 2013.

[30] J. W. Chi, M. Brady, N. R. Moore, and J. A. Schnabel. Segmentation of the bladder wall using coupled level set methods. In *2011 IEEE International Symposium on Biomedical Imaging: From Nano to Macro*, pages 1653–1656, March 2011.

[31] G. Chen, H. Lin, X. Wen, T. Wang, and R. Chen. Study of image processing for mr diffusion weighed image. In *2010 3rd International Congress on Image and Signal Processing*, volume 3, pages 1465–1468, Oct 2010.

[32] H. y. Jiang and Z. y. Cheng. Segmentation of pulmonary nodules based on statistic features of wavelet coefficients and dual level sets. In *2007 IEEE/ICME International Conference on Complex Medical Engineering*, pages 648–651, May 2007.

[33] Huibin Chang, Xue-Cheng Tai, Li-Lian Wang, and Danping Yang. Convergence rate of overlapping domain decomposition methods for the rudin-osher-fatemi model based on a dual formulation. *SIAM J. Imaging Sciences*, 8:564–591, 2015.

[34] Fatema A. Albalooshi and Vijayan K. Asari. A self-organizing lattice boltzmann active contour (solbac) approach for fast and robust object region segmentation. *2015 IEEE International Conference on Image Processing (ICIP)*, pages 1329–1333, 2015.

[35] J. W. Chi, M. Brady, N. R. Moore, and J. A. Schnabel. Segmentation of the bladder wall using coupled level set methods. In *2011 IEEE International Symposium on Biomedical Imaging: From Nano to Macro*, pages 1653–1656, March 2011.

[36] Hao Zhang, Lihong Li, Hongbin Zhu, Hao Han, Bowen Song, and Zhengrong Liang. Integration of 3d scale-based pseudo-enhancement correction and partial volume image segmentation for improving electronic colon cleansing in ct colonography. *Journal of X-ray science and technology*, 22 2:271–83, 2014.

[37] Christian Gout, Carole Le Guyader, and Luminita A. Vese. Segmentation under geometrical conditions using geodesic active contours and interpolation using level set methods. *Numerical Algorithms*, 39:155–173, 2004.

[38] Shawn Lankton and Allen Tannenbaum. Localizing region-based active contours. *IEEE Transactions on Image Processing*, 17:2029–2039, 2008.

[39] C. Li, C.-Y. Kao, J.C. Gore, and Z. Ding. Minimization of region-scalable fitting energy for image segmentation. *IEEE Transactions on Image Processing*, 17(10):1940–1949, 2008.

[40] Vicent Caselles, Ron Kimmel, and Guillermo Sapiro. Geodesic active contours. *International Journal of Computer Vision*, 22:61–79, 1995.

[41] National Laboratory for Scientific Computing. *Single ACM Evolution*., http://virtual01.lncc.br/~giraldi/Snakes/snakest0.exe, 2001.

[42] National Laboratory for Scientific Computing. *Dual ACM Evolution*. http://virtual01.lncc.br/~giraldi/Snakes/Dual-Level-Set.avi, 2005.

[43] A. K. Jain and A. Vailaya. Shaped-based retrieval: a case study with trademark image database. *Pattern Recognition*, 31:1369–1390, 1998.

[44] L. Rada and Ke Chen. A new variational model with dual level set functions for selective segmentation. *Communications in Computational Physics*, 12(1):261–283, 2012.

[45] XiaoHong Han, Xiaoyan Xiong, and Fu Duan. A new method for image segmentation based on bp neural network and gravitational search algorithm enhanced by cat chaotic mapping. *Applied Intelligence*, 43:855–873, 2015.

[46] X. S. Zhu, Q. S. Sun, and D. S. Xia. Adaptive active contour model integrating global and local image fitting energy. *Journal of Image and Graphics*, 17(9):1109–1114, 2012.

[47] Jin Yu Liu, Zheng Ning Zhang, and He Meng Yang. A variational level set remote sensing sar image segmentation approach for oil spill detecting based on fuzzy cluster. In *Materials and Engineering Technology*, volume 719 of *Applied Mechanics and Materials*, pages 1049–1055. Trans Tech Publications, 2 2015.

[48] Yi Zhang and Xiaozhong Yang. Accelerated additive operator splitting

schemes for nonlinear diffusion filtering. *2010 International Conference on Biomedical Engineering and Computer Science*, pages 1–4, 2010.

[49] Troy Farncombe and Kris Iniewski. *Medical Imaging: Technology and Applications*. CRC Press, Inc., Boca Raton, FL, USA, 1st edition, 2017.

[50] Peter Kovesi. Symmetry and asymmetry from local phase. In *Tenth Australian Joint Conference on Artificial Intelligence*, pages 2–4, 1997.

[51] G. Strang and T. Nguyen. *wavelets and Filter Banks*. Wellesley-Cambridge Press, 1996.

[52] Jasjit S. Suri, Kecheng Liu, Sameer Singh, Swamy Laxminarayan, Xiaolan Zeng, and Laura Reden. Shape recovery algorithms using level sets in 2-d/3-d medical imagery: a state-of-the-art review. *IEEE Transactions on Information Technology in Biomedicine*, 6(1):8–28, 2002.

[53] G. A. Giraldi, E. Strauss, and A. F. Oliveira. Dual-T-Snakes model for medical imaging segmentation. *Pattern Recognition Letters*, 24(7):993–1003, 2003.

[54] A.X. Falcão, B.S. da Cunha, and R.A. Lotufo. Design of connected operators using the image foresting transform. In *SPIE on Medical Imaging*, volume 4322, pages 468–479, February 2001.

[55] R. Nock and F. Nielsen. Statistical region merging. *IEEE Trans. on Patt. Analysis and Mach. Intell.*, 26:1452–1458, 2004.

[56] G. A. Giraldi, E. Strauss, and A. A. F. Oliveira. A boundary extraction method based on dual-t-snakes and dynamic programming. *In Proc. of IEEE Computer Society Conference on Computer Vision and Pattern Recognition, CVPR'2000*, 2000.

[57] Jean-Jacques Rousselle, Nicole Vincent, and Nicolas Verbeke. Genetic algorithm to set active contour. In Nicolai Petkov and Michel A. Westenberg, editors, *Computer Analysis of Images and Patterns*, pages 345–352, Berlin, Heidelberg, 2003. Springer Berlin Heidelberg.

[58] G. A. Giraldi. *T-Snakes Duais e Inicialização de Modelos Deformáveis*. PhD thesis, Departamento de Engenharia de Sistemas e Computação - COPPE - UFRJ. Web Site (In portuguese): http://virtual01.lncc.br/~giraldi/Tese/index.html, 2000.

[59] B. Wang, X. Yuan, X. Gao, X. Li, and D. Tao. A hybrid level set with semantic shape constraint for object segmentation. *IEEE Transactions on Cybernetics*, pages 1–2, 2018.

[60] G. A. Giraldi, L. M. G. Gonçalvez, and A. A. F. Oliveira. Dual topologically adaptable snakes. *In Proceedings of the Fifth Joint Conference on Information Sciences (JCIS' 2000) - Third International Conference on Computer Vision, Pattern Recognition, and Image Processing*, 2:103–106, 2000.